Hydrogen Production at a NiO Photocathode Based on a Ruthenium Dye-Cobalt Diimine Dioxime Catalyst Assembly: Insights from Advanced Spectroscopy and Post-operando Characterization

Emmanouil Giannoudis, Sébastian Bold, Caroline Müller, Alexander Schwab, Jakob Bruhnke, Nicolas Queyriaux, Corinne Gablin, Didier Léonard, Christine Saint-Pierre, Didier Gasparutto, et al.

Hydrogen production at a NiO photocathode based on a ruthenium dye – cobalt diimine dioxime catalyst assembly: insights from advanced spectroscopy and post-operando characterization

E. Giannoudis,[‡a] S. Bold,[‡a,b,c,d] C. Müller,[b,c,d] A. Schwab,[b] J. Bruhnke,[b] N. Queyriaux,[a] C. Gablin,[e] D. Leonard,[e] C. Saint-Pierre,[f] D. Gasparutto,[f] D. Aldakov,[f] S. Kupfer,[b] V. Artero,[a] B. Dietzek,[b,c,d] M. Chavarot-Kerlidou[,a]*

a. Univ. Grenoble Alpes, CNRS, CEA, IRIG, Laboratoire de Chimie et Biologie des Métaux, Université Grenoble Alpes, 17 rue des Martyrs, F-38000 Grenoble, France.

b. Institute of Physical Chemistry and Abbe Center of Photonics, Friedrich Schiller University Jena, Helmholtzweg 4, 07743 Jena, Germany.

c. Department Functional Interfaces, Leibniz Institute of Photonic Technology Jena (IPHT), Albert-Einstein-Straße 9, 07745 Jena, Germany.

d. Center for Energy and Environmental Chemistry Jena (CEEC Jena), Friedrich Schiller University Jena, Philosophenweg 8, 07743 Jena, Germany.

e. Univ Lyon, CNRS, Université Claude Bernard Lyon 1, Institut des Sciences Analytiques, UMR 5280, 5, rue de la Doua, F-69100 Villeurbanne, France.

f. Univ. Grenoble Alpes, CNRS, CEA IRIG, SyMMES, F-38000 Grenoble, France.

Keywords.

Solar fuels, hydrogen, photoelectrochemistry, dye-sensitized, cobalt catalyst.

Abstract.

The production of hydrogen by efficient, low-cost and integrated photo-electrochemical water splitting processes represents an important target for the ecological transition. This challenge can be addressed thanks to bioinspired chemistry and artificial photosynthesis approaches, through designing dye-sensitized photocathodes for hydrogen production incorporating bioinspired first row transition metal-based catalysts. The present work describes the preparation and photoelectrochemical characterization of a NiO photocathode sensitized with a phosphonate-derivatized ruthenium tris-diimine photosensitizer covalently linked to a cobalt diimine dioxime hydrogen-evolving catalyst. Under simulated AM 1.5G irradiation, hydrogen is produced with photocurrent densities reaching 84 ± 7 $\mu A.cm^{-2}$, which is among the highest values reported so far for dye-sensitized photocathodes with surface-immobilized catalysts. Thanks to the unique combination of advanced spectroscopy and surface characterization techniques, the fast desorption of the dyad from the NiO electrode and the low yield of electron transfer to the catalyst resulting in the Co demetallation from the diimine dioxime framework were identified as the main barriers limiting the performances and the stability of the system. This work therefore paves the way for a more rational design of molecular photocathodes for solar fuel production and represents a further step towards the development of sustainable processes for the production of hydrogen from solar and water.

Introduction.

Production of hydrogen (H_2) through sunlight-driven water splitting is one relevant strategy to meet the challenges of a carbon-neutral economy. Among the various technological approaches proposed to date, water splitting photoelectrochemical cells are appealing as integrated, low-cost and scalable devices.[1-3] Dye-sensitized photoelectrochemical cells (DS-PECs) can more specifically elaborate on the well-established dye-sensitized solar cell (DSSC) technology to

build active photoelectrodes via the immobilization of molecular components, *i.e.* light-harvesting units and catalysts, at the surface of transparent conducting oxide films.[4-7] In addition, they benefit from the recent achievements in the field of bioinspired catalysis for energy-relevant applications to integrate appropriate first raw transition metal-based catalysts for hydrogen production.[8-10] Proof of concept for this approach was recently provided with the first DS-PECs based on such bioinspired catalysts and built in a tandem configuration reproducing the Z scheme of Photosynthesis.[11-13]

Various electrode architectures have been successfully described to assemble molecular H_2-evolving catalysts (cobalt, nickel or iron complexes, typically) with light-harvesting units (organic dyes, porphyrin or ruthenium tris-diimine complexes) at the surface of a suitable mesoporous semi-conducting oxide film.[14-16] They typically rely on the anchoring of supramolecular or covalent dye-catalyst assemblies,[17-22] the co-immobilisation of both components,[11-13, 23-27] or alternatively, a layer-by-layer assembly strategy.[28-32] In addition to this structural diversity, a wide range of activity conditions (nature and pH of the electrolyte, applied potential, light source and intensity…) were reported, preventing the establishment of clear structure-activity relationships although the latter would be highly beneficial to rationally improve the photocathode molecular design. Yet, all examples of functional H_2-evolving dye-sensitized photocathodes so far reported display overall low performances in terms of photocurrent densities, turnover numbers (TON) and, in some cases, faradaic efficiencies (F.E.).

NiO is the main p-type semi-conductor employed in these studies and various procedures have been employed to prepare mesoporous nanostructured films with thicknesses varying from a few hundreds of nm to a few μm.[33] One important limitation with these NiO electrodes relates to the fast primary charge recombination processes, reported to occur on the picosecond timescale, being thus competitive with charge accumulation and catalysis.[15, 25, 30, 32] These

investigations rely, however, on ultrafast spectroscopic measurements made on *dry* sensitized films, which questions the relevance of these kinetic data to rationalize the low photoelectrochemical activity. Indeed, the groups of Papanikolas and Hammarström independently reported bias-dependent charge recombination kinetics for Ru tris-diimine-sensitized NiO electrodes.[34-35] Applying a cathodic potential to the film was shown to fill the intra-bandgap states at the origin of the fast recombination processes, with a subsequent increase of the charge separation state lifetime from the ps to the μs timescale.

In addition to these kinetic limitations, photocurrents rapidly decrease within a few hours of activity, raising important questions about the stability of previously-reported molecular photocathodes.[11-13, 17-32] Comprehensive studies providing a deep understanding of the deactivation pathways at work with the photocatalytic systems remain scarce, however, in the literature; techniques allowing to provide mass-related molecular information about the species present at the surface of the film, such as ToF-SIMS, have in particular not been employed in that context, apart in a collaborative study between the groups of M. Price and E. Gibson[18] or by our group.[23, 36] Deciphering, thanks to a combination of advanced techniques, the structural and electronic factors limiting the activity and affecting the stability of these photocathodes is thus of paramount importance to develop dye-sensitized water splitting devices able to meet robustness and efficiency.

We previously reported a series of hydrogen-evolving NiO photocathodes featuring covalent dye – cobalt catalyst assemblies prepared by a modular click chemistry coupling strategy.[19-20, 37-38] A standardized protocol was established to assess the photoelectrochemical performances under identical conditions, thus allowing a rational comparison of the activity of the different dyads. In these studies, we exploited in particular the well-known properties of push-pull organic dyes to achieve a unidirectional electron transfer cascade from the electrode to the catalytic center; their degradation under reductive conditions was however identified as a main

issue for stability.[38] This was further supported by transient absorption – spectroelectrochemistry (TA-SEC) measurements recorded on the sensitized films at the operando potential, which allowed to detect the formation of the Co^{I} catalytically-active species albeit in very low yield, thus leading to the accumulation and degradation of the reduced dye at the surface of the film.[38] Here, we report on the synthesis and characterization of a novel dyad, **RuP$_4$-Co**, featuring a ruthenium tris-diiimine photosensitizer substituted by four methylphosphonate anchoring groups,[39] covalently linked to the cobalt diimine-dioxime H_2-evolving catalyst.[40] Compared to the previous systems relying on the same catalyst,[19-20, 22, 37-38] significant improvements in the photocurrent density (four to six-fold increase) and F.E. (seven fold increase) for hydrogen production were achieved with the corresponding NiO-based **RuP$_4$-Co**-sensitized photocathode (Figure 1). Moreover, the main parameters affecting the performance of our system were identified thanks to a comprehensive analysis of the photoelectrochemical activity combined with TA-SEC measurements and quantum chemical simulations on one hand and in-depth post-operando characterizations based on a combination of XPS, UV-vis and mass spectrometry-related techniques on the other hand.

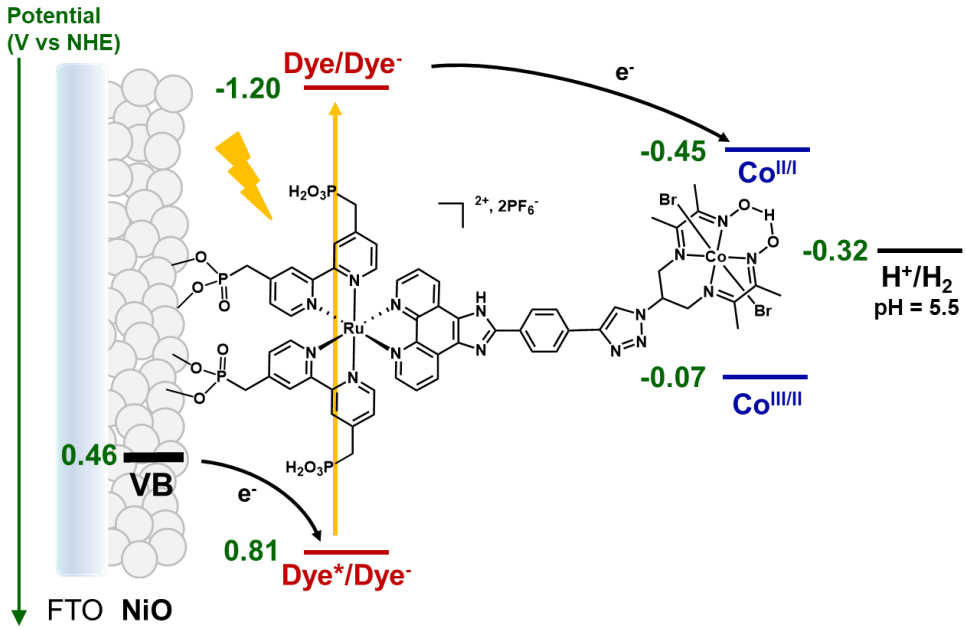

Figure 1. Energy diagram and working principle of the **RuP$_4$-Co**-sensitized NiO photocathode at pH 5.5 (arbitrary representation of the phosphonate anchoring mode onto NiO). The NiO

valence band edge potential was estimated from the 0.37 V *vs* NHE value previously reported at pH 7.[41]

Results and discussion.

Synthesis of ***RuP$_4^{OEt}$-Co*** *and characterization in solution.*

RuP$_4^{OEt}$-Co was synthesized by a copper-catalyzed azide-alkyne cycloaddition (CuAAC) coupling between the alkyne-substituted dye precursor **RuP$_4^{OEt}$-EPIP**[39] and the azido-functionalized copper diimine dioxime complex,[42] followed by a transmetallation step from Cu to Co, according to our previously-reported procedures.[19-20] Acid-base titrations revealed that the dye precursor and the dyad were isolated under their imidazole-protonated form (Figure S2). Full synthetic details and characterizations are provided in the Supporting Information.

The electronic and redox properties of **RuP$_4^{OEt}$-Co** were first investigated in solution and were compared to the ones individually determined for the two components **RuP$_4^{OEt}$-EPIP** and $[Co(DO)(DOH)N_3pnBr_2]$[43] (**CoN$_3$**). Its UV-vis absorption spectrum recorded in acetonitrile (Figure S3) is characteristic for a ruthenium tris-diimine complex, with a broad absorption band centered at 460 nm and attributed to the metal-to-ligand charge transfer (^{1}MLCT) transition. Quantum chemical simulations on the structurally closely related **RuP$_4^{OMe}$-Co** assign three ^{1}MLCT transitions to this absorption feature, *i.e.* into the S_6, S_8 and S_{10} state respective, with mixed contributions from the ruthenium to the bipyridine ligands as well as to the phenanthroline-based ligand (see quantum chemical simulations section below). In the UV region, intense ligand-centered π-π* absorption bands are observed between 270 and 350 nm, together with a small contribution from the cobalt center at 300 nm, by comparison with the spectrum recorded for **CoN$_3$**. The redox properties are summarized in Table 1 and the cyclic voltammograms are displayed in Figure S4. On the anodic scan, **RuP$_4^{OEt}$-Co** exhibits a reversible Ru^{III}/Ru^{II} process at +0.89 V *vs* $Fc^{+/0}$, which is not significantly affected by the coupling. On the cathodic scan, five reduction processes take place between −0.60 and −2.45

V *vs* $Fc^{+/0}$, corresponding to the two successive reduction of the cobalt center, Co^{III}/Co^{II} (E_{pc} = −0.60 V *vs* $Fc^{+/0}$) and Co^{II}/Co^{I} ($E_{1/2}$ = −0.98 V *vs* $Fc^{+/0}$), then the reduction of the three diimine ligands in the Ru^{II} coordination sphere. Overall, the electronic and redox properties of **RuP_4^{OEt}-Co** can be simply described as the superimposition of those of its individual **RuP_4^{OEt}** and **Co** components, thus underlining that the dye and the catalyst moieties are electronically decoupled in the ground state. Similar observations were previously made for a ruthenium-copper[42] and the push-pull organic dye-based **T1-Co** dyad,[20] and are frequently reported in the literature for triazole-based assemblies.[44-46]

Table 1. Redox properties[a] of **Co-N_3**, **RuP_4^{OEt}-EPIP** and **RuP_4^{OEt}-Co** recorded in acetonitrile.

	***E*ox[b] Ru^{III}/Ru^{II}**	***E*red$_1$[c] $Co^{III/II}$**	***E*red$_2$[b] $Co^{II/I}$**	***E*red$_3$[b] Ru^{II}/Ru^{II}-$L^{\bullet-}$**	ΔG_{inj}[d]	ΔG_1[e]	ΔG_2[f]
Co-N_3	—	−0.60 (−0.07)	−1.01 (−0.48)	—	—	—	—
RuP_4^{OEt}-EPIP	+0.92 (+1.45)	—	—	−1.71 (−1.18)	−0.36	—	—
RuP_4-Co	+0.89 (+1.42)	−0.60 (−0.07)	−0.98 (−0.45)	−1.73 (−1.20)	−0.34	−1.13	−0.75

a- In V *vs* $Fc^{+/0}$ and in V *vs* NHE (value in brackets). Redox potentials converted from $Fc^{+/0}$ to NHE, considering $E°(Fc^{+/0})$ = +0.53 V *vs* NHE in acetonitrile.
b- ½(E_{pc} + E_{pa}).
c- E_{pc}.
d- In eV. Gibbs free energy for hole injection ΔG_{inj} = e[E_{VB}(NiO) − E(PS*/PS^-)]; with E_{VB}(NiO) = +0.46 V *vs* NHE at pH 5.5[20] and E(PS*/PS^-) = E(PS/PS^-) + E_{00} (see Table S1 for E_{00} values).
e- In eV. Gibbs free energy for electron transfer from the reduced dye to the Co^{III} catalyst ΔG_1 = e[E(Ru^{II}/Ru^{II}-$L^{\bullet-}$) − E(Co^{III}/Co^{II})].
f- In eV. Gibbs free energy for electron transfer from the reduced dye to the Co^{II} catalyst ΔG_2 = e[E(Ru^{II}/Ru^{II}-$L^{\bullet-}$) − E(Co^{II}/Co^{I})].

Furthermore, the dye and dyad excited state dynamics were investigated by nanosecond (ns) time-resolved absorption and emission spectroscopies, on the as-synthesized complexes as well as on their neutral imidazole form (generated in-situ by the addition of one equivalent of triethylamine). Emission lifetimes of 170 and 160 ns were determined for **RuP_4^{OEt}-EPIP** and **RuP_4^{OEt}-Co**, respectively (Table S1, Figure S5). In addition, upon excitation at 410 nm, very similar transient absorption spectra were recorded for both complexes irrespective of the protonation state of the imidazole ring (Figures S6 & S7): a ground state bleach is observed at 460 nm together with a broad and structureless absorption above 500 nm, assigned to the

absorption of the ^{3}MLCT excited state. The latter decays concomitantly with the ground state recovery over a few hundreds of ns, supporting the absence of any additional process, *i.e.* no intramolecular electron transfer process from the ruthenium excited state to the Co^{III} center occurs in **RuP_4^{OEt}-Co**, as previously reported for **T1-Co**.[47]

NiO film sensitization and dyad loading quantification.

Homemade F108-templated NiO films[20] were soaked for 24 hours in a methanolic solution of the **RuP_4-Co** dyad (or the **RuP_4-EPIP** dye) after deprotection of the phosphonate anchoring groups (see SI for experimental details). The amount of dyad loaded on the film was determined by UV-vis absorption spectroscopy after desorption of the freshly-sensitized NiO film in a 1 M phenylphosphonic acid methanolic solution,[17, 48] using the molar extinction coefficient of the MLCT band at 460 nm (Figure S8). An average dyad loading of 5.2 ± 0.8 nmol·cm^{-2} was obtained (12 independent samples; Table S2), which is slightly lower than the ones we previously reported for related ruthenium tetraphosphonate dyes,[36] but in agreement with the lower thickness of the spin-coated films employed here (700 nm to 1 μm, Figure S9). The dyad loading was systematically quantified on one half of a freshly-sensitized NiO film, the other half being employed for the photoelectrochemical experiments. Hence, the amount of dyad grafted on the electrode was precisely known for each sample and was used to calculate the TONs for hydrogen production activity (see below).

*Photoelectrochemical performances of **RuP_4-Co**-sensitized NiO photocathodes.*

Photoelectrochemical measurements were conducted in aqueous conditions at pH 5.5 (0.1 M 2-(*N*-morpholino)ethanesulfonic acid (MES) / 0.1 M NaCl buffer),[19-20] using a **RuP_4-Co**-sensitized NiO film as working electrode in a three-electrode setup. We previously showed that the activity of the cobalt diimine dioxime catalyst is optimal at mildly acidic pHs,[49] and no H_2

evolution could be detected at pH 7 for this catalyst anchored onto multiwalled carbon nanotubes.[43] Linear sweep voltammograms recorded under dark, light and chopped light irradiation (filtered Xenon lamp, 400 – 800 nm, 65 mW·cm^{-2} equivalent to 1 sun) revealed the generation of cathodic photocurrents, steadily increasing from +0.9 V to 0 V *vs* RHE (Figure S10, Table S3). In order to correlate them to some photoelectrocatalytic hydrogen production activity, two hours chronoamperometric measurements (Figure S11) were performed under continuous light irradiation at an applied potential of +0.14 V *vs* RHE (−0.4 V *vs* Ag/AgCl); at the end of the experiment, the amount of hydrogen was quantified both in the headspace and in solution, according to our previously reported procedure.[19] Under these conditions, 28 ± 2 nmol · cm^{-2} (5 ± 1 TON) of hydrogen were produced with 24 ± 5 % faradaic efficiency (F.E.) for the NiO|**RuCo** photocathode (Table 2).

Table 2. Figures of merit determined from the two-hour chronoamperometric measurements (full set of experimental data in Table S4).

Irradiation	Photocathode	$n(H_2)$[a] (nmol·cm^{-2})	Charge[b] (mC · cm^{-2})	F.E.[c] (%)	TON_{Co}[d]
400-800 nm	NiO	1 ± 1	3 ± 1	5 ± 2	—
	NiO|**Ru-EPIP**	4 ± 1	9 ± 1	9 ± 1	—
	NiO|**RuCo**	28 ± 2	24 ± 6	24 ± 5	5 ± 1
Simulated AM 1.5G	NiO	5 ± 0	8 ± 1	13 ± 1	—
	NiO|**Ru-EPIP**	10 ± 4	10 ± 4	22 ± 2	—
	NiO|**RuCo**	60 ± 9	45 ± 6	26 ± 7	13 ± 2

a- Total amount of H_2 produced, quantified in solution and in the headspace (detailed values in Table S4), divided by the geometric surface area (measured for each single film).
b- Charge passed during the course of the two hours chronoamperometric measurement divided by the geometric surface area (measured for each single film).
c- Faradaic efficiency for hydrogen production.
d- Turnover number (calculated with the dyad loading determined for each single film).

Replacing the 400 nm cut-off filter by an AM 1.5G one, which better simulates solar irradiation, proved to be highly beneficial for the photoelectrochemical performances of **RuP_4-Co**. A significant increase in the photocurrent density is observed (Figure 2, top), reaching up to 97 μA · cm^{-2} (Table S3). This is due to a beneficial contribution from the absorption in the UV part of the spectrum, as previously reported for homogeneous photocatalytic hydrogen

production based on ruthenium trisdiimine photosensitizers.[50-51] Hence, 60 ± 9 nmol · cm^{-2} of hydrogen (26 ± 7 % F.E.) were produced during the course of a two hours chronoamperometric measurement under these optimized irradiation conditions (Figures 2 & S12), corresponding to 13 ± 2 TONs (Table 2).

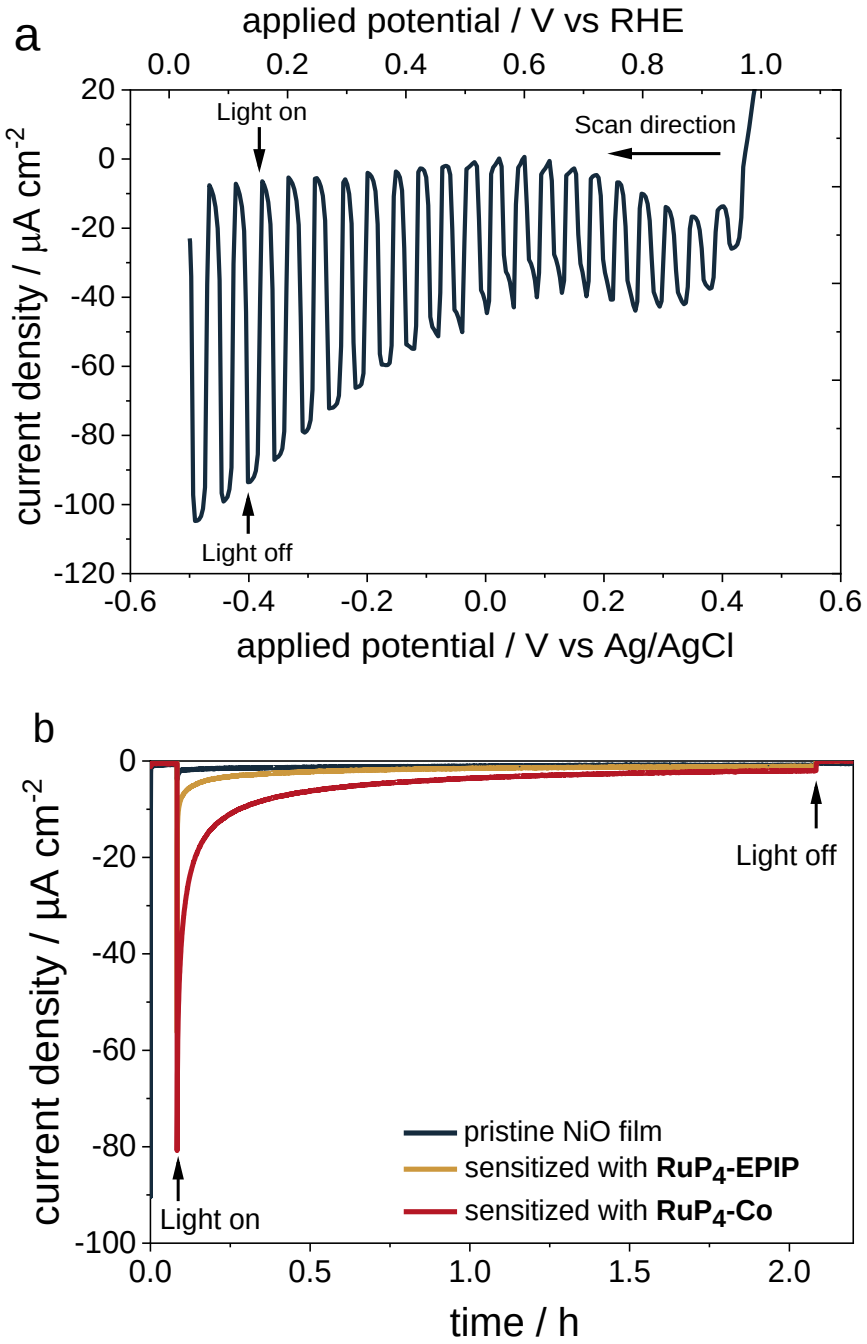

Figure 2. *a*) Linear sweep voltammogram recorded on a **RuP$_4$-Co**-sensitized NiO electrode under chopped light irradiation (simulated AM 1.5G, IR filtered) in MES 0.1 M/NaCl 0.1M supporting electrolyte at pH 5.5. *b*) Photocurrent densities recorded during the course of a two-hour chronoamperometric measurement under continuous light irradiation (simulated AM 1.5G, IR filtered) at an applied potential of + 0.14 V *vs* RHE.

Whatever the irradiation setup, control experiments using either non-sensitized NiO films or **RuP$_4$-EPIP**-sensitized ones display significantly lower photocurrents compared to the **RuP$_4$-Co** photocathode (Figure 2, bottom and Figure S11). Moreover, in the absence of the Co catalyst at the surface of the film, the amount of hydrogen produced by the dye-sensitized photocathode is 6 to 7 times lower for similar dye loadings (Tables 2 & S4).[52] These results clearly support a cobalt-based mechanism for the observed H_2 evolving activity.

The performances of the **RuP$_4$-Co** photocathode proved to be superior to the ones we previously reported for the **T1-Co** photocathode based on an organic push-pull dye, which displayed a TON of less than five and a 10 % F.E. for hydrogen production, under identical conditions.[19-20,38] To further investigate the role played by the light-harvesting unit and its electronic nature, UV-vis monitored photolysis experiments were performed on **RuP$_4^{OEt}$-Co** and **T1^{OtBu}-Co** at 4.5 x 10^{-5} M in a CH_3CN/TEOA (90:10) solution (Figure S13).[53] Upon visible light irradiation, the characteristic two-band spectrum of the Co^I species[54] builds up between 500 and 800 nm, albeit with a final absorption 2 to 3 times higher for **RuP$_4^{OEt}$-Co** (reached after 30 minutes) compared to **T1^{OtBu}-Co** (reached after 60 min of irradiation). These observations thus suggest that the photoinduced generation of the Co^I state, entry point to the cobalt-centered H_2-evolving catalytic cycle,[40] might be more efficient with **RuP$_4^{OEt}$-Co** than with **T1^{OtBu}-Co**. Yet, the TON achieved by the cobalt diimine dioxime catalyst under the photoelectrochemical conditions reported here is very low compared to the TON of 300 previously obtained under homogeneous photocatalytic conditions,[55] or the 7,000 (TON) achieved by the Co(DO)(DOH)pn-based electrocatalytic nanomaterial under close aqueous conditions.[43]

TONs being affected by both the kinetic and the stability over time of the system, we re-examined the LSV measurements in order to extract initial turnover frequency (TOF) values of activity. From the photocurrent densities at +0.14 V *vs* RHE under visible light irradiation

(Table 3), a TOF of 0.11 $nmol_{e-} \cdot nmol_{\mathbf{RuCo}}^{-1} \cdot s^{-1}$ was determined for the **RuP$_4$-Co**-sensitized film (*i.e.* each grafted **RuP$_4$-Co** dyad efficiently relays one electron every 9 s), which is five times higher than for the **T1-Co**-sensitized film (0.02 $nmol_{e-} \cdot nmol_{\mathbf{T1Co}}^{-1} \cdot s^{-1}$). Including UV irradiation provides a track for improvement, by increasing the Ru dye light absorption efficiency via its upper excited state levels. This results in a slightly increased TOF, reaching 0.18 $nmol_{e-} \cdot nmol_{\mathbf{RuCo}}^{-1} \cdot s^{-1}$ (Table 3), and in turn, a more than doubled TON (TON_{Co}: 13 *vs* 5, see Table 2) over 2 hours irradiation when simulated AM 1.5G irradiation conditions are employed compared to visible light irradiation. We could thus increase the initial TOF by varying either the nature of the light-harvesting unit or the irradiation conditions (all other conditions being strictly equal). This demonstrates that, at the beginning of the two-hour chronoamperometric measurement, the cobalt-centered catalytic activity is not the limiting parameter of the system. This is further supported by the TOF value of 1.3 s^{-1} (equal to 2.6 $nmol_{e-} \cdot nmol_{\mathbf{Co}}^{-1} \cdot s^{-1}$) determined from the specific rate of H_2 evolution previously measured for **Co** anchored onto multi-walled carbon nanotubes (MWCNT).[43]

Table 3. Kinetic data at +0.14 V *vs* RHE from the LSV measurements (see the full set of experimental data in Table S3) and comparison with the activity of the previously-reported MWCNT-based cathode material functionalized with **Co**.

Irradiation	(Photo)cathode	Photocurrent density (j; $\mu A \cdot cm^{-2}$)[a]	TOF (electrons) ($nmol_{e-} \cdot nmol_{\mathbf{dyad}}^{-1} \cdot s^{-1}$)[b]	TOF (H_2) ($TON \cdot s^{-1}$)
400-800 nm	NiO|**T1Co**[c]	15[c]	0.02	0.01[d]
	NiO|**RuP$_4$-Co**	58 ± 11	0.11 ± 0.03	0.055[d]
Simulated AM 1.5G	NiO|**RuP$_4$-Co**	84 ± 7	0.18 ± 0.03	0.09[d]
—	MWCNT|**Co**[e]	—	—	1.3[f]

a- Dark current substracted.
b- Converted from j using TOF = j / $n \cdot F \cdot \Gamma$, with j in $A \cdot cm^{-2}$ (1 A = 1 $C \cdot s^{-1}$), Γ in $mol \cdot cm^{-2}$, n = 1 electron transferred, F = 96 485 $C \cdot mol^{-1}$.
c- Data taken from our previous study.[20]
d- Expected TOF(H_2) if H_2 is produced with a F.E. of 100%.
e- Data taken from our previous study.[43]
f- Obtained by dividing the specific rate of H_2 evolution at −0.6V *vs* RHE (6 $nmol_{H2} \cdot s^{-1} \cdot cm^{-2}$) by the catalyst loading (4.5 $nmol \cdot cm^{-2}$)

Conclusively, these observations strongly suggest that the **RuP$_4$-Co** photocathode suffers from *i*) kinetic issues, *i.e*. the catalytic center is not correctly supplied with electrons to achieve fast catalysis, *ii*) stability issues, which is further supported by the very fast photocurrent decrease observed during the course of the chronoamperometric measurements (> 90 % loss within the first hour of activity, Figure 2). These two points are addressed below in-depth, thanks to time-resolved spectroscopic studies on the sensitized films supported by quantum chemical calculations and post-operando characterization, respectively.

Investigation of the ultrafast electron transfer processes.

The kinetics of the light-induced processes occurring at the dye-sensitized photocathode interface were investigated by transient absorption spectroelectrochemistry (TA-SEC). TA spectra were recorded in a home-built spectroelectrochemical cell (see details in SI) at different cathodic potentials applied to the film, in order to determine the influence of the applied potential on the hole injection and charge recombination dynamics. Previous studies by the groups of J. M. Papanikolas[34] and L. Hammarström[35] indeed highlighted the pronounced dependence of the charge-separated state lifetime on the potential applied to NiO films sensitized by model Ru dyes, while our own preliminary work focused on the effect of potential on the excited-state reactivity in organic dye-catalyst dyads.[38, 47] Measurements were carried out in a dry acetonitrile electrolyte to get rid of any catalytic turnover in order to accumulate and detect the Co^I species. TA spectra were recorded at the open-circuit potential (OCP) and at −0.74 V *vs* $Fc^{+/0}$, which corresponds to the operando potential in the photoelectrochemical activity tests (−0.4 V *vs* Ag/AgCl); a previous study showed that this potential is sufficient to generate the Co^{II} state of the cobalt catalyst at the surface of the film.[23] In addition, control experiments were also carried out *i*) at −1.15 V *vs* $Fc^{+/0}$, where the cobalt catalyst is already in its Co^I state and as a consequence, electron transfer is no longer thermodynamically possible,

and *ii*) on films sensitized with **RuP$_4$-EPIP** instead of **RuP$_4$-Co**, at all of the aforementioned potentials.

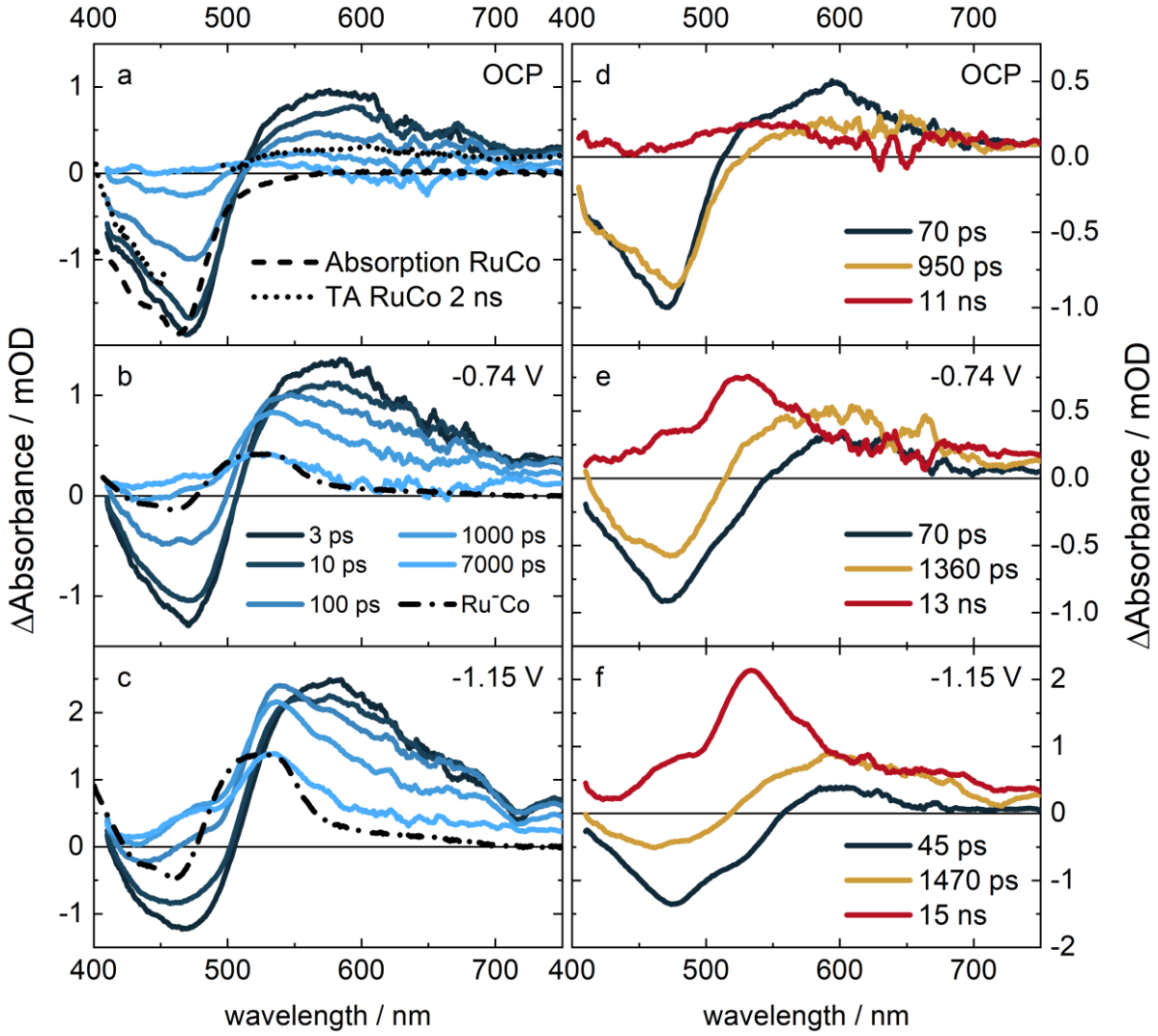

Figure 3. TA-SEC spectra (a-c) and decay-associated spectra (d-f) obtained with a three-component exponential fit of **RuP$_4$-Co**-sensitized NiO films at early delays up to 7 ns at (a,d) OCP, (b,e) −0.74 V and (c,f) −1.15 V *vs* $Fc^{+/0}$ applied potential. For clarity, the spectra were integrated over ±10% of the given times and smoothed by a 10-point adjacent averaging. The raw data without smoothing are depicted in Figure S21. The inverted absorption spectrum of **RuP$_4^{OEt}$-Co** in ACN (dashed line), the TA spectrum of **RuP$_4^{OEt}$-Co** in ACN at 2 ns time delay (dotted line) and the scaled differential absorption spectrum upon one-electron reduction of the Ru complex in **RuP$_4^{OEt}$-Co** (dashed-dotted line) are given for comparison.

TA spectra of NiO films sensitized with **RuP$_4$-EPIP** and **RuP$_4$-Co** show the same general features: At early times, a spectrum with ground-state bleach (GSB) at 480 nm and excited-state absorption (ESA) around 590 nm is observed, corresponding to the MLCT state (Figure 3, Figures S14-S17). At OCP, this spectrum decays almost completely within the time window

of the experiment (7 ns) except for a weak positive band centered at 520 nm. At negative applied potentials, however, this minor feature develops into a broad and long-lived signal (between 540 – 480 nm), completely overwriting the GSB. The band at 540 nm is characteristic for the one-electron reduced Ru dye (dashed-dotted lines in Figures 3 and S18). The band at 480 nm is tentatively assigned to oxidized Ni centers produced by hole injection (HI),[56-57] leading to the assignment of this spectrum to the primary charge-separated state produced by HI from the excited dye into the NiO film ($NiO^{+}|Ru^{I}$). A tri-exponential fit of the experimental data yields the time constants for HI ranging from 67 ps (at OCP) to 31 ps (at −1.15 V *vs* $Fc^{+/0}$) for **RuP_4-EPIP** and from 67 ps (at OCP) to 45 ps (at −1.15 V *vs* $Fc^{+/0}$) for **RuP_4-Co** (Table S5), *i.e.* becoming faster and more pronounced at more negative potential applied (Figure 3 d-f). In addition, the initial GSB signal at 480 nm becomes weaker while the initial reduced dye absorption signal at 540 nm is increased (Figure S19); this suggests that an additional ultrafast (< 2 ps) HI process occurs when a cathodic potential is applied to the film. HI is ultimately followed by charge recombination (CR), which is also strongly affected by the applied potential: at OCP, CR is characterized by a time constant of tens of picoseconds, while at cathodic potentials, the charge separated state lives for more than 7 ns, as previously observed for a ruthenium dye-sensitized NiO photocathode.[34]

In parallel to HI, there is a process with a characteristic time constant of about 1 ns, *i.e.* τ_2 = 950-1470 ps, which shows the spectral signature of a MLCT decay to the ground state (concerted loss of GSB and ESA). This decay reflects a direct deactivation of excited molecules, which do not undergo HI. This process might be associated with self-quenching of tightly packed dyads on the NiO surface.[58] Alternatively, a combination of rate-limiting HI and rapid CR can account for the same spectral features. The lower amplitude and slower rate for this component at more negative applied potentials supports this assignment: HI is faster, decreasing

the amount of long-lived ^{3}MLCT states, and CR is slowed down by the lower concentration of holes on the NiO surface.

Most importantly, in the time window up to 7 ns, the TA spectra of **RuP$_4$-Co** do not show any spectral indication of charge transfer to the cobalt catalyst unit. Such a charge transfer would be observable as an increasing absorption band between 550 and 750 nm produced by the Co^I state (Figure S18), which is not present in the fs-TA-SEC spectra recorded for **RuP$_4$-Co** at −0.74 V *vs* $Fc^{+/0}$. Since thermal electron transfer in triazole-bridged dyads has been shown to occur on the ns-µs time scale,[59-63] especially for a related H_2-evolving photocathode sensitized with a push-pull organic dye-cobalt catalyst covalent assembly,[38] we performed TA experiments under identical conditions in the ns-µs time scale. The data recorded in this time range are spectrally identical to the last spectra recorded in the fs-TA-SEC experiment and decay without any spectral changes, with 15% of the initial signal still left after 45 µs (Figures 4, S20 & S21). The decay occurs in a non-exponential fashion as typical for charge recombination reactions in molecularly functionalized NiO photoelectrodes.[34-36, 64-65] Quantitative kinetic analysis of the ns-TA data using a three-component exponential fit yields similar lifetimes at −0.74 V and at −1.15 V *vs* $Fc^{+/0}$ ($\tau_{3,1} \approx 90$ ns, $\tau_{3,2} \approx 1.4$ µs, $\tau_{3,3} \approx 14$ µs with an average lifetime of $\tau_{ave} = 4$ µs for **RuP$_4$-Co** at -0.74 V *vs* $Fc^{+/0}$, Figure S20 & S21, Table S5).

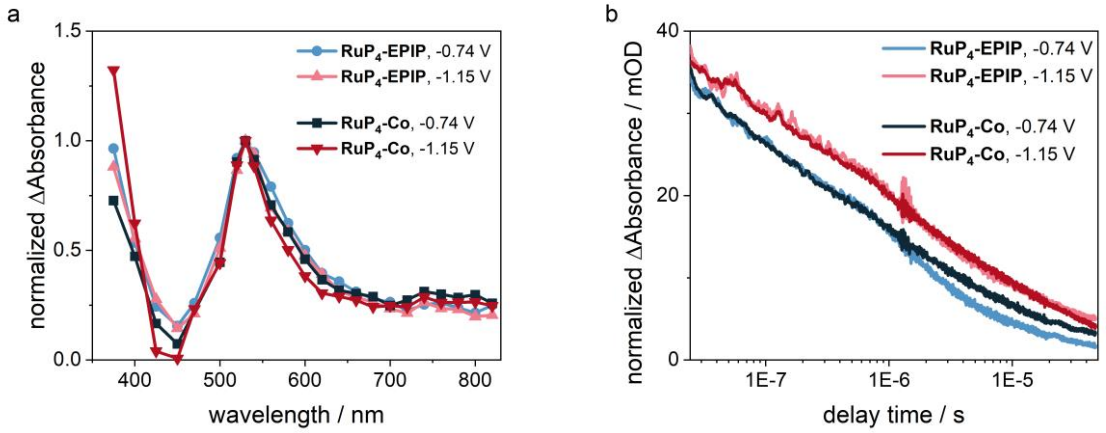

Figure 4. a) TA spectra of **RuP$_4$-EPIP-** and **RuP$_4$-Co-**sensitized NiO films at −0.74 V and −1.15 V *vs* $Fc^{+/0}$ applied potential at 100 ns time delay, normalized to signal at 530 nm. b) Kinetic traces at 530 nm of the same data, averaged from 520 to 540 nm and normalized at 30 ns to the signal of **RuP$_4$-Co** at the respective potential.

Applying a cathodic potential to the film thus leads to an increase of up to 5 orders of magnitude of the lifetime of the charge-separated state (up to 14 μs) compared to the situation without applied potential (OCP, a few hundreds of ps). However, in spite of this long-lived charge-separated state, no direct evidence for electron transfer to the cobalt catalyst[38] could be observed on the ns to μs time window: indeed, within the experimental signal to noise, the expected spectral signature of the Co^{I} state between 600 and 800 nm was not detected on the TA spectra of **RuP_4-Co**-sensitized NiO films at −0.74 V *vs* $Fc^{+/0}$ (Figure 4), and the decay kinetics of the reduced Ru moiety were not accelerated in comparison to **RuP_4-EPIP**-sensitized films (Figure 4). Based on the ratio of the extinction coefficients of the reduced dye and of the Co^{I} state from the UV-Vis SEC experiment (Figure S18), the growth of a signal with a 9.0 mOD intensity is expected if Co^{I} is formed with 100 % yield from the primary charge-separated state already formed at the beginning of the ns-TA-SEC experiment. Considering the experimental noise of 0.5 mOD, the limit of detection at a signal to noise ratio of 2:1 is estimated to be 1 mOD, corresponding to a yield of formation of the Co^{I} species of 12 %. The absence of any spectral evidence supporting the formation of Co^{I} thus clearly indicates that the electron transfer efficiency from the reduced dye to the catalytic center lies below this detection limit. In consequence, the TOF for hydrogen production is rather low as the active Co^{I} species is not formed efficiently. The light-induced processes occurring for the **RuCo**-sensitized film at the operando potential are summarized in Figure 5.

Figure 5. Jablonski diagram summarizing the light-induced processes occurring for **RuP_4-Co**-sensitized NiO films at −0.74 V *vs* $Fc^{+/0}$ (equivalent to the −0.4 V *vs* Ag/AgCl used in the photoelectrochemical experiments). Electron density is depicted in blue, while holes are depicted in red. Dashed arrows indicate the processes that have not been detected.

To further investigate the photoinduced electron transfer processes at a molecular level, we performed a series of quantum chemical simulations at the density functional (DFT) and time-dependent DFT level of theory for **Ru-Co** as well as for **RuP_4^{OMe}-Co**. These simulations aim to elucidate the excited states populated upon photoexcitation, the subsequent reduction of the

excited intermediate (*i.e.* hole injection upon NiO immobilization of **RuP$_4$-Co**) as well as the sequential intramolecular electron transfer steps, and, finally to the catalytic active species. Although, the singly reduced Co^{II} is already obtained at the applied operando potential, the performed (TD)DFT simulations involve a potential light-driven Co^{III}/Co^{II} reduction as well as the second Co^{II}/Co^{I} reduction – investigated in-depth by the TA-SEC experiments.

Initially, the nature of the electronic transitions underlying the absorption spectrum of **Ru-Co** as well as of **RuP$_4^{OEt}$-Co** was assessed using TDDFT, while the structural and electronic properties of **RuP$_4^{OEt}$-Co** were obtained for the computationally less demanding **RuP$_4^{OMe}$-Co** complex. Both complexes feature a broad absorption band between 500 and 400 nm, which stems mainly from the excitation into three ^{1}MLCT states: Both lower energy MLCT transitions, predicted at roughly 460 (2.7 eV; **RuP$_4^{OEt}$-Co**: S_7 and **Ru-Co**: S_6) and 445 nm (2.8 eV; **RuP$_4^{OEt}$-Co** and **Ru-Co**: S_9), are of mixed electronic character and feature excitations from the Ru atom to the bpy as well as to the phen ligand spheres. In contrast, the higher energy transition at ca. 435 nm (2.85 eV; **RuP$_4^{OEt}$-Co** and **Ru-Co**: S_{10}) is of pure $MLCT_{bpy}$ nature, for details see Figure 6a and Figure S22 as well as Tables S6 and S7 in the Supporting Information. The following computational analysis will be focused exclusively on **Ru-Co**. As highlighted above, the singly reduced **Ru-Co** species (*i.e.* Co^{II}) is already obtained at the applied operando potential. However, such species may be obtained as well in a light-driven fashion, which will be evaluated in the following based on computational modelling. Therefore, 480-nm excitation into the MLCT band of the non-reduced **Ru-Co** – into the S_6, S_9 and S_{10} ^{1}MLCT states – may lead subsequently to an ultrafast intersystem crossing and the population of various close-lying ^{3}MLCT states, see Figure 6a and Tables S6 and S7. Consequently, electrochemical reduction may yield the singly reduced doublet Ru^{II} species of **Ru-Co**, while the accessory charge is either localized on one bpy ligand or on the phen moiety, *i.e.*, in the lowest π^*_{bpy} or π^*_{phen} molecular orbital, respectively. Energetically, bpy-based reduction, as illustrated by the spin densities of

D_0 (bpy reduction) in Figure 6c, is slightly more favourable with respect to the reduction of the phen moiety (see spin density of D_1). However, thermally induced distortions, *i.e.*, elongation of the Co-Br bond lengths, may stabilized the initially unfavourable Co-centered reduction (D_4 in Figure 6c, Co^{II}) leading to the semi-charged catalytic center. DFT predicts a driving force (ΔE) of -0.51 eV for this intramolecular electron transfer, while an activation energy (E_A) of approximately 0.37 eV was predicted along a linear-interpolated internal coordinate connecting the equilibrium geometries of the phen-based and the Co-based reductions using pysisyphus,[66] an efficient external optimizer written in Python – that is also aware of excited states. In line with previous computational studies, in which dissociation of the halide ligands becomes favourable upon reduction,[67-68] we observe a considerable elongation of the Co-Br bonds from 2.418 and 2.421 Å (phen-based reduction state) to 2.539 and 2.572 Å (Co-based reduction state; Table S8). Therefore, three different Co^{II} structures were used in the quantum chemical simulations related to the photoinduced electron transfer leading eventually to the catalytically active Co^{I} species: a first one with two Br^- ligands, the Co^{II}-based catalyst structure proposed by Artero and co-workers,[67] with the two Br^- ligands being dissociated and one ACN (solvent) molecule coordinated and the Co^{II} structure with two ACN coordinated ligands as calculated by Hammes-Shiffer and coworkers.[68] In the following, only the computational results obtained for the Co^{II} structure with two ACN molecules (**Ru-Co(ACN)$_2$**) are described; results obtained for the Co^{II} structure with one solvent molecule (**Ru-Co(ACN)**) as well as for the catalyst with two bromide ligands (**Ru-Co**) are discussed in the supporting information. Excitation of this singly reduced **^{2}[Ru-Co(ACN)$_2$]**, as shown in Figure 6d, yields very similar mixed $^2MLCT_{bpy}$ and $^2MLCT_{phen}$ transitions (see D_{21}, D_{41} and D_{45} in Figure 6d as well as D36 and D38 in Tables S6 and S7) in the visible region, which was to be expected as the initial electronic configuration of the Ru^{II} photosensitizer is recovered. However, a partial contribution of the bridging ligand is predicted by TDDFT, see D_{21} and D_{45} in Figure 6d. In case of the doubly

reduced photocatalyst, ^{1}**[Ru-Co(ACN)$_2$]**, exclusively singlet species were considered as the fully charged Co^{I} formally features a low-spin d^8 configuration. Figure 6f illustrates the intramolecular electron transfer pathways and the accessory charge localization, *i.e.* with the second reduction centered on one bpy ligand (S_2), on the phen-moiety (S_3) and on the Co catalyst (S_0) – the fully charged and catalytic active Co^{I} species. Analogous as for the first electron transfer (Figure 6c), bpy and phen-based reductions are isoenergetic, while a pronounced mixing of bpy and phen contributions hampered the identified and optimized of charge-separated Co^{II} species, see SI for details. However, the second reduction (Co^{II}/Co^{I}) proceeds with a thermodynamical unfavorable driving force of approximately +0.36 eV, thus hampering the formation of the catalytic active Co^{I} species. However, population of the Co^{I} redox state leads in consequence to the dissociation of one ACN ligand (Table S8; $d(CoACN_1)$ = 3.821 Å) leading to **Ru-Co(ACN)** and, thus substantially stabilizing the catalytic active species (Figure S23i).[67] Noteworthy, the driving force for the $Co^{II/I}$ reduction was found to be highly sensitive to the Co^{II}'s coordination sphere. An increased electron density at the Co^{II} site, as given by two coordinated bromide ligands, yields an even more unfavorable driving force of +0.39 eV, while a decreased electron density, as given by the pentacoordinates Co^{II} species (one ACN), yields a strong driving force of -1.15 eV for the Co^{I} formation. Experimentally, a driving force of -0.75 eV was determined for the Co^{II}/Co^{I} reduction, recall Table 1. Presumably, this discrepancy reflects a coordination environment at the cobalt center with one coordinated and one loosely bound solvent molecule which cannot be fully described based on the present computational approach. Metadynamic simulations are the method of choice to describe such scenario, unfortunately the computational demand prevents an application in the present case. Further details with respect to computational results and the impact of the cobalt coordination sphere on its redox properties are collected in the Supporting Information.

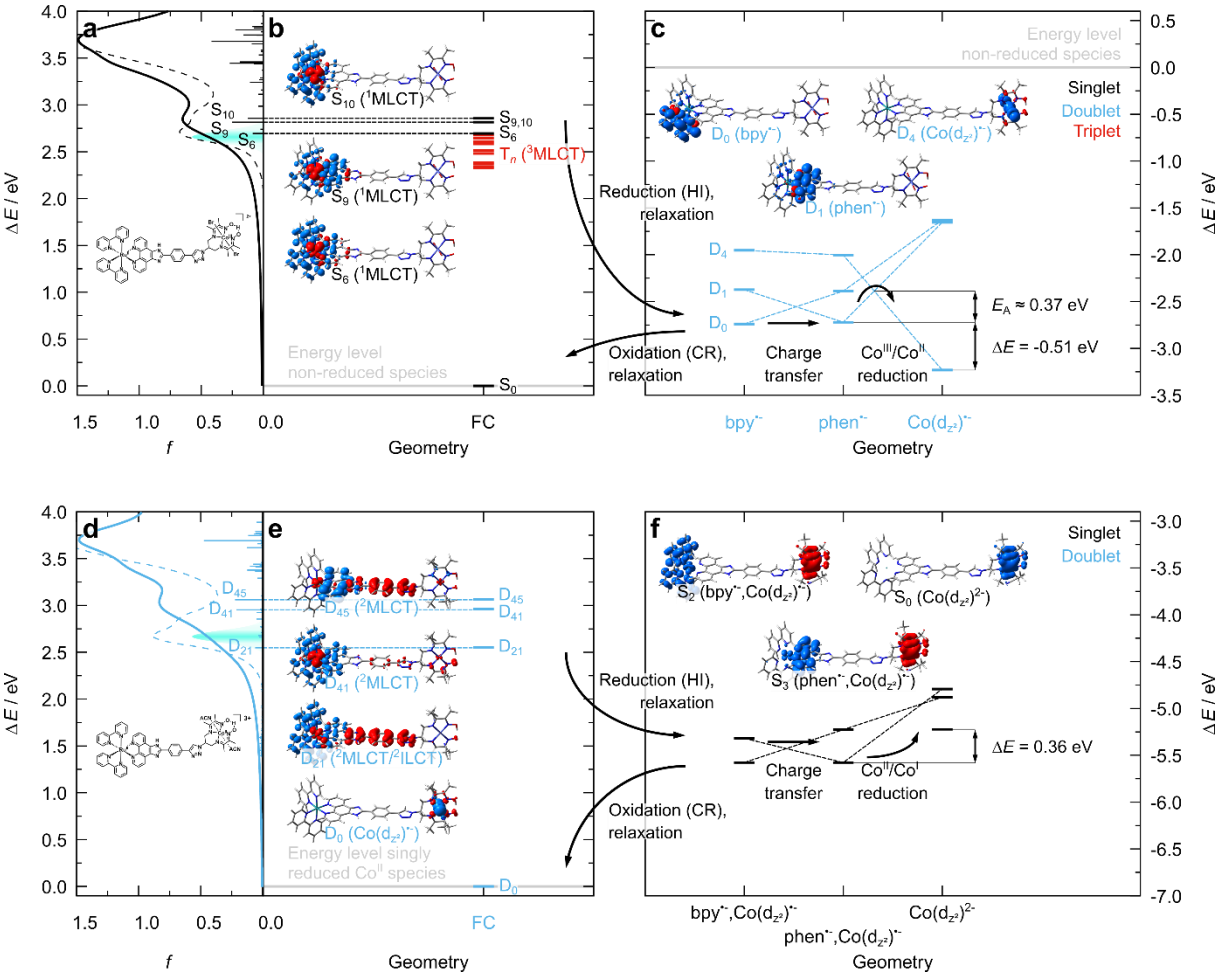

Figure 6. a) Singlet UV-vis absorption spectrum of **Ru-Co** (experimental data: dashed line, simulated data: solid line) and, b), energy levels of prominent singlet and triplet excitations in the Franck-Condon geometry (FC, singlet ground state equilibrium). c) Singly reduced states with excess charge localized on one bpy ligand ($bpy^{\bullet-}$), on the phen ligand ($phen^{\bullet-}$) and at the catalytic center – leading to the partially charged Co^{II} species with semi-occupied d_{z^2}(Co) orbital. All states are shown in their respective equilibrium structures. d) Spin-allowed doublet excitations contributing to the UV-vis absorption spectrum of **Ru-Co(ACN)$_2$** (both Br-dissociated and two ACN coordinated; simulated data: solid line). e) Energy levels of prominent doublet excitations in the Franck-Condon geometry (doublet ground state equilibrium of Co^{II} species shown in c)). f) Doubly reduced states with one excess charge localized at the Co, *i.e.* Co^{II} species, and the other excess charge on one bpy ligand ($bpy^{\bullet-}$), on the phen ligand ($phen^{\bullet-}$) and at the catalytic center – leading to the fully charged Co^{I} species with doubly occupied d_{z^2}(Co) orbital. All states are shown in their respective equilibrium structures. Quantum chemical results were obtained at the (time-dependent) density functional level of theory (B3LYP/def2-svp) including D3BJ dispersion correction and solvent effects (ACN) by a polarizable continuum model. Electronic nature of prominent transitions is shown by charge density differences, charge localization in the respective electronic ground state of opened-shell species is illustrated by the spin density. The highest-occupied molecular orbital of the Co^{I} is shown in f). Singlet, doublet, and triplet states are shown in black, blue, and red, respectively.

The reasons why the formation of the catalytically competent Co^{I} state isn't experimentally observed whereas electron transfer from the reduced dye is predicted to occur with a high driving force are still unclear at that stage. A possible explanation might involve a small electronic coupling between the redox states involved in the formation of the Co^{I} species, *e.g.* as shown previously for triazole-based linkers.[69] We recently made a similar observation for a related dyad based on a cobalt tetraazamacrocyclic catalyst covalently linked to a push-pull organic dye: the formation of the Co^{I} state of the catalyst could be detected within 20 ns after laser pulse excitation but with a yield far from unity, a lot of reduced dye remaining present at the surface of the film on the μs time window.[38] This therefore raises questions regarding *i*) the choice of a covalent dye-catalyst assembly based on a CuAAC coupling, the role played by the triazole unit in the photoinduced electron transfer processes presenting some controversy in the literature;[70] *ii*) the influence of the dyad anchoring within the pores of the NiO film, which might strongly affect the parameters controlling the thermal electron process to the catalytic center due to some conformational or topological constraints, thus leaving only a small fraction of dyads active for hydrogen production. Future joint synthetic-spectroscopic-theoretical studies of the consortium will focus on the impact of the electronic coupling on the electron transfer kinetics in detail as shown recently by semi-classical Marcus theory and quantum dynamics for a ruthenium-cobalt photocatalyst model.[71]

Post-operando characterization.

X-ray photoelectron spectroscopy (XPS) and time-of-flight secondary ion mass spectrometry (ToF-SIMS) were first employed to characterize the structural modifications undergone by the photocathode during the course of the two hours chronoamperometric experiment. The survey XPS spectrum of a post-operando **RuP$_4$-Co**-sensitized NiO film is shown in Figure 7a, together with the ones recorded on the same freshly-sensitized film and on a bare NiO film, for

comparison purposes. Surface modification by **RuP_4-Co** is confirmed by the appearance of new peaks at 132.4, 280.6, and 400.1 eV, characteristic for the P 2p, Ru 3d and N 1s core levels, respectively (Figures 7 & S24). The chemical state of Ni is not modified upon sensitization, nor post-operando (Figure S25); in particular, the formation of Ni^0 (typically observed at 852.6 eV) is not detected here. The relative concentration of these elements is decreased post-operando (Table S9), indicating that 30 to 50 % of the dyad is released in solution during the course of the photoelectrochemical activity measurement. The Co^{III} catalyst is detected at 780.4 eV (Co 2p3/2 core level) for the freshly-sensitized film (Figure 7b): even though this signal is masked by the overlapping Ni Auger background complicating its quantification, upon the deconvolution it is possible to observe the Co signal (see inset in Figure 7b). The latter is in perfect agreement with the XPS analyses previously reported for the same catalyst co-immobilised onto NiO with a push-pull organic dye[23] or anchored onto MWCNTs.[43] Furthermore, this signal is absent (or lies below the detection limit) in the spectrum recorded post-operando, suggesting that the loss of Co is more important compared to Ru. Desorption of the dyad from the surface of the NiO film is also evidenced by ToF-SIMS analysis. Comparison of the positive mode spectra recorded on a freshly-sensitized film and the same one post-operando (Figure S26) clearly show that, while some peaks attributed to the dyad are still significantly present (Ru-containing signatures such as the peak detected at m/z = 616.01), others can hardly be detected at the end of two hours photoelectrocatalytic experiment (typically the Co-containing signatures such as the peak detected at m/z = 659.17). In the negative mode spectra, the detection of various $Ni_aP_bO_cH_d^-$ fragments (Figure S27) provides evidence for the covalent attachment of the dyad on the surface of the NiO electrode through the formation of inorganic ester bonds, as previously observed for related systems.[36] These peaks are also detected post-operando.

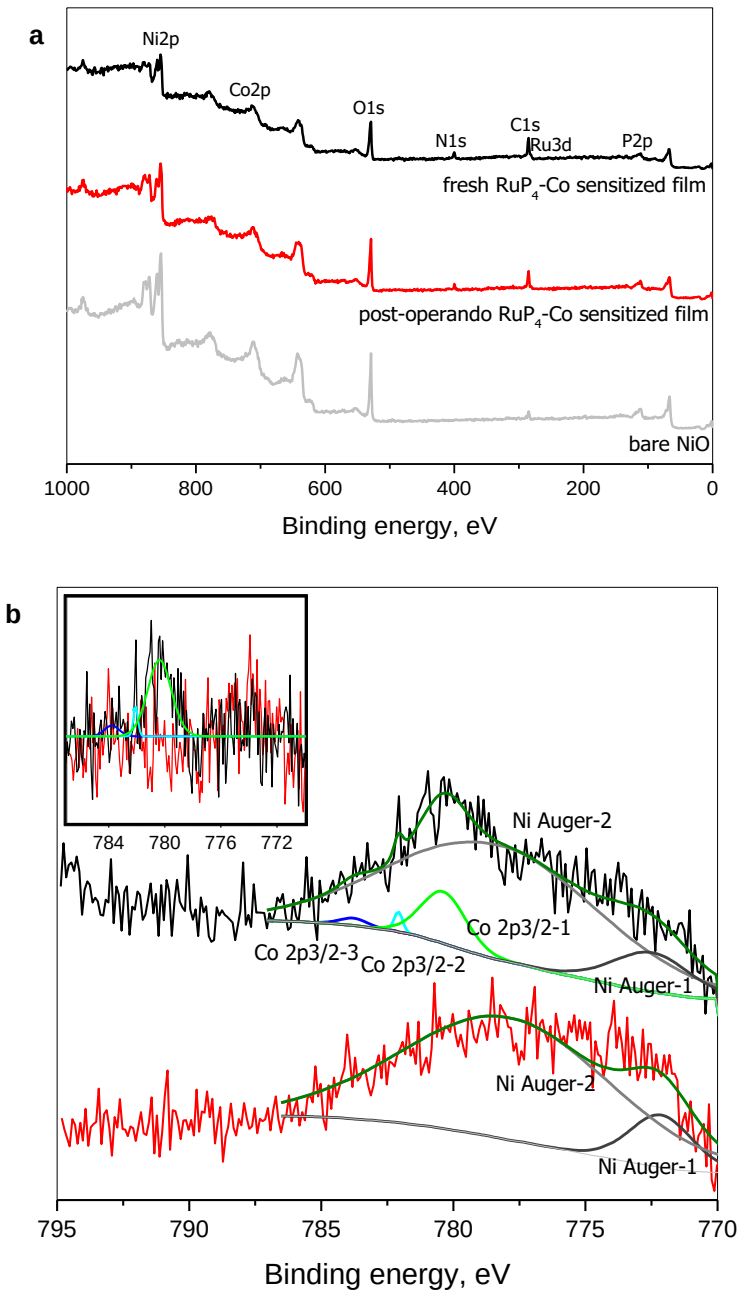

Figure 7. a) Survey XPS spectra recorded on a pristine NiO film (grey), a fresh **RuP$_4$-Co**-sensitized film (black) and the same film post-operando (red). b) XPS core-level spectra of the Co 2p3/2 region and corresponding deconvolution of the signals (Inset: overlap of the spectra corrected for the Ni Auger background).

In parallel to these two techniques directly probing the sensitized film at the end of the chronoamperometric measurements, desorption of the remaining molecular species from the surface of the film was also undertaken and the desorption solution analyzed by UV-vis absorption spectroscopy. For all analyzed samples, the post-operando UV-vis spectra revealed

an important decrease in absorption compared to those recorded for the other half of the film freshly desorbed (Figure 8), giving an average percentage of dyad desorption of 80 % (independent of the irradiation conditions, see Table S4). Thus, the presence of the four phosphonate anchors failed to stabilize the grafting onto the NiO film surface. Working at pH 5.5 for an optimal H_2-evolving activity whereas phosphonate grafting is reported to be stable below pH 5[72-73] might rationalize this behaviour. In addition to UV-vis spectroscopy, MALDI-ToF mass spectrometry was employed to provide further information regarding the fate of the molecular dyad. The spectrum recorded after desorption of a freshly-sensitized film (Figure S28) is quasi superimposable to the **RuP$_4$-Co** reference spectrum, with a main peak at m/z = 1448 attributed to the $[M\text{-}2PF_6\text{-}2Br]^{4+}$ ion together with additional fragmentation peaks such as the loss of one oxygen atom at m/z = 1432.[74] By contrast, at the end of the two hours PEC experiment, these characteristic peaks have disappeared and the spectrum displays a single peak at m/z = 1224 (Figure 8). Its isotopic pattern is in agreement with the one calculated for the diamino derivative of the dyad (structure presented in Figure 8), which could be formed via a degradation pathway involving the hydrolysis of the cobalt diimine dioxime catalytic core during the course of the PEC experiment.

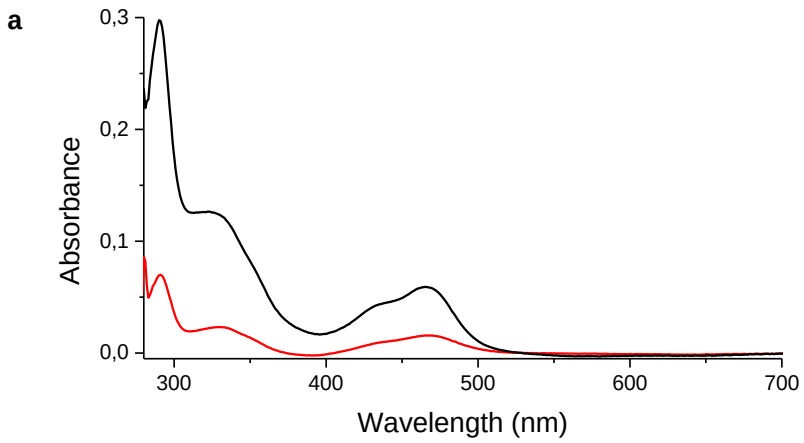

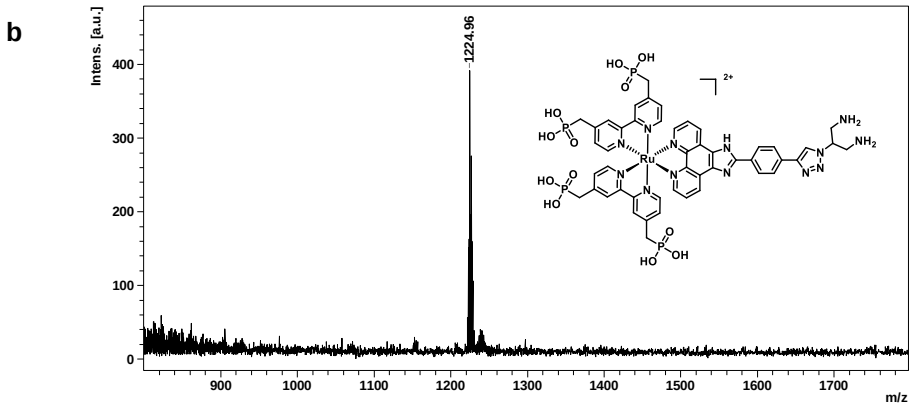

Figure 8. a) UV-vis absorption spectra of desorption solutions (1 M phenylphosphonic acid in methanol) of a fresh **RuP$_4$-Co**-sensitized NiO film (black) and the same film post-operando (red). b) MALDI-ToF mass spectrum recorded on the post-operando desorption solution and structure of the molecular assembly corresponding to the peak at 1224.

To verify how these stability issues affect the faradaic efficiency of the system, a chronoamperometric test was run over half an hour instead of two hours, 59 nmol·cm^{-2} of hydrogen being produced with a 72 % F.E. (Table S4). This clearly highlights that, during the first minutes of activity under continuous irradiation, the charges are selectively used to produce H_2, albeit this selectivity rapidly decrease over time to yield the 25 % F.E. recorded after two hours. The performances of the **RuP$_4$-Co** photocathode are thus strongly limited by the relatively fast dyad desorption from the surface of the NiO film, together with the lack of stability of the diimine dioxime coordination sphere under the photoelectrochemical conditions of activity, *i.e*. in an aqueous electrolyte at pH 5.5. The latter point sharply contrasts with the previously reported activity for **Co** covalently anchored onto a nanostructured carbon-based electrode, continuously producing H_2 for 4 hours with a near-quantitative F.E. under very close aqueous conditions (acetate buffer, pH 4.5).[43] We believe such a difference in stability is related to the supply of electrons to the catalytic center, which is optimized in the MWCNT/Co electrocatalytic material by contrast to the NiO|**RuCo** photocathode. The consequence of the low electron transfer efficiency identified above is a slow charge accumulation process at the cobalt center; this might leave enough time for the degradation of some catalytic intermediates through cobalt demetallation and subsequent hydrolysis of the diimine bonds of the ligand.

Cobalt demetallation was previously reported to be the dominating deactivation pathway for a related cobaloxime-based photocathode, preventing any catalytic activity.[32]

Conclusion.

In conclusion, the preparation and characterization of a novel NiO photocathode integrating the cobalt diimine dioxime H_2-evolving catalyst covalently linked by CuAAC coupling to a ruthenium tris-diimine light-harvesting unit is described. Photocurrent densities of 84 ± 7 $\mu A \cdot cm^{-2}$ were recorded under simulated AM 1.5G irradiation, which is among the highest values reported so far for dye-sensitized photocathodes with surface-immobilized catalysts. Hydrogen was produced with an unprecedented 72 % F.E. during the first 30 minutes of the chronoamperometric measurements, but this activity declined rapidly over two hours. A comprehensive analysis of the photoelectrochemical data established that catalysis at the cobalt center is not the kinetically limiting process, the initial TOF being increased when varying either the irradiation conditions or the nature of the light-harvesting unit, *i.e.* it is five times higher herein compared to the one previously-reported with the push-pull organic dye **T1**, all other conditions being strictly equal. The interfacial electron transfer dynamics were further investigated by transient absorption measurements recorded with the operando potential applied to the film (TA-SEC) as well as by quantum chemical simulations addressing the stepwise intramolecular electron transfer processes among the various redox intermediates eventually leading to the formation of the catalytic active species. The low yield of the thermally-activated electron transfer from the reduced dye to the catalyst was identified as the main kinetic bottleneck, and not the primary recombination between the reduced dye and the hole in NiO as often called on to explain the low performances reported so far for H_2-evolving dye-sensitized NiO photocathodes. In addition, a combination of post-operando characterization techniques, namely XPS, ToF-SIMS and UV-vis spectroscopy combined to MALDI-ToF mass

spectrometry allowed to identify the hydrolytic degradation of the catalytic center, together with an important percentage of dyad released in solution, as the two main stability issues. This study thus paves the way toward the construction of more performant H_2-evolving dye-sensitized photocathodes in view of their integration in tandem water-splitting PECs. Work should focus in particular on the design of molecular assemblies allowing to more efficiently shuttle electrons from the dye to the catalytic center. The integration of robust molecular catalysts, typically the cobalt-polypyridyl[75-78] or the cobalt tetraazamacrocyclic[38, 79] complexes, will also be instrumental to increase the long-term stability. Finally, various surface chemistry strategies can be applied to stabilize the molecular grafting onto the electrode, such as the ALD deposition of a thin layer of alumina,[80] or the use of silatrane anchors that are hydrolytically stable over a wide range of pHs.[81-82]

ASSOCIATED CONTENT

Supporting Information. Experimental details regarding the synthesis and characterization in solution of the **RuP_4^{OEt}-Co** dyad can be found in the Supporting Information together with additional (photo)electrochemical, spectroscopic and simulation data.

AUTHOR INFORMATION

Corresponding Author

* Murielle Chavarot-Kerlidou; E-mail: murielle.chavarot-kerlidou@cea.fr

Author Contributions

The manuscript was written through contributions of all authors. All authors have given approval to the final version of the manuscript. ‡These authors contributed equally.

Funding Sources

This work was supported by the European Commission's Seventh Framework Program (FP7/2007-2013) under grant agreement n° 306398 (FP7-IDEAS-ERC, Project PhotocatH_2ode), the Deutsche Forschungsgemeinschaft (German Science Foundation, PHOTOACC project, Grant No. KU 3933/2-1) and the French National Research Agency in the framework of the "Investissements d'avenir" program (ANR-15-IDEX-02, Labex ARCANE and CBH-EURGS, ANR-17-EURE-0003) and the Franco-German University.

ACKNOWLEDGMENT

Adina Morozan is acknowledged for the SEM measurements. Jacques Pecaut (CEA/DRF/IRIG/DIESE/SyMMES) is acknowledged for the ESI-MS measurements. This work was supported by the European Commission's Seventh Framework Program (FP7/2007-2013) under grant agreement n° 306398 (FP7-IDEAS-ERC, Project PhotocatH_2ode), the Deutsche Forschungsgemeinschaft (German Science Foundation, PHOTOACC project, Grant No. KU 3933/2-1) and the French National Research Agency in the framework of the "Investissements d'avenir" program *(*ANR-15-IDEX-02, Labex ARCANE and CBH-EUR-GS, ANR-17-EURE-0003). S.B. wants to thank the Franco-German University for the cotutelle thesis funding support. We want to thank the workshop of the IPHT Jena for their help in building the spectroscopy cell.

REFERENCES

(1) Li, F.; Yang, H.; Li, W.; Sun, L. Device Fabrication for Water Oxidation, Hydrogen Generation, and CO₂ Reduction via Molecular Engineering. *Joule* **2018,** *2* (1), 36-60, DOI: 10.1016/j.joule.2017.10.012.

(2) McKone, J. R.; Lewis, N. S.; Gray, H. B. Will Solar-Driven Water-Splitting Devices See the Light of Day? *Chem. Mater.* **2014,** *26* (1), 407-414, DOI: 10.1021/cm4021518.

(3) Walter, M. G.; Warren, E. L.; McKone, J. R.; Boettcher, S. W.; Mi, Q.; Santori, E. A.; Lewis, N. S. Solar Water Splitting Cells. *Chem. Rev.* **2010,** *110*, 6446-6473.

(4) Yun, S.; Vlachopoulos, N.; Qurashi, A.; Ahmad, S.; Hagfeldt, A. Dye Sensitized Photoelectrolysis Cells. *Chem. Soc. Rev.* **2019,** *48* (14), 3705-3722, DOI: 10.1039/C8CS00987B.

(5) Zhang, S.; Ye, H.; Hua, J.; Tian, H. Recent Advances in Dye-Sensitized Photoelectrochemical Cells for Water Splitting. *EnergyChem* **2019,** *1* (3), 100015, DOI: https://doi.org/10.1016/j.enchem.2019.100015.

(6) Xu, P.; McCool, N. S.; Mallouk, T. E. Water Splitting Dye-Sensitized Solar Cells. *Nano Today* **2017,** *14*, 42-58, DOI: https://doi.org/10.1016/j.nantod.2017.04.009.

(7) Brennaman, M. K.; Dillon, R. J.; Alibabaei, L.; Gish, M. K.; Dares, C. J.; Ashford, D. L.; House, R. L.; Meyer, G. J.; Papanikolas, J. M.; Meyer, T. J. Finding the Way to Solar Fuels with Dye-Sensitized Photoelectrosynthesis Cells. *J. Am. Chem. Soc.* **2016,** *138* (40), 13085-13102, DOI: 10.1021/jacs.6b06466.

(8) Dalle, K. E.; Warnan, J.; Leung, J. J.; Reuillard, B.; Karmel, I. S.; Reisner, E. Electro- and Solar-Driven Fuel Synthesis with First Row Transition Metal Complexes. *Chem. Rev.* **2019,** *119* (4), 2752-2875, DOI: 10.1021/acs.chemrev.8b00392.

(9) Artero, V. Bioinspired Catalytic Materials for Energy-Relevant Conversions. *Nature Energy* **2017,** *2* (9), 17131, DOI: 10.1038/nenergy.2017.131.

(10) Berardi, S.; Drouet, S.; Francas, L.; Gimbert-Surinach, C.; Guttentag, M.; Richmond, C.; Stoll, T.; Llobet, A. Molecular Artificial Photosynthesis. *Chem. Soc. Rev.* **2014,** *43* (22), 7501-7519, DOI: 10.1039/C3CS60405E.

(11) Windle, C. D.; Kumagai, H.; Higashi, M.; Brisse, R.; Bold, S.; Jousselme, B.; Chavarot-Kerlidou, M.; Maeda, K.; Abe, R.; Ishitani, O.; Artero, V. Earth-Abundant Molecular Z-Scheme Photoelectrochemical Cell for Overall Water-Splitting. *J. Am. Chem. Soc.* **2019,** *141* (24), 9593-9602, DOI: 10.1021/jacs.9b02521.

(12) Li, F.; Fan, K.; Xu, B.; Gabrielsson, E.; Daniel, Q.; Li, L.; Sun, L. Organic Dye-Sensitized Tandem Photoelectrochemical Cell for Light Driven Total Water Splitting. *J. Am. Chem. Soc.* **2015,** *137* (28), 9153-9159, DOI: 10.1021/jacs.5b04856.

(13) Fan, K.; Li, F.; Wang, L.; Daniel, Q.; Gabrielsson, E.; Sun, L. Pt-free Tandem Molecular Photoelectrochemical Cells for Water Splitting Driven by Visible Light. *Phys. Chem. Chem. Phys.* **2014,** *16* (46), 25234-25240, DOI: 10.1039/C4CP04489D.

(14) Wu, H.-L.; Li, X.-B.; Tung, C.-H.; Wu, L.-Z. Sensitized Photocathodes: Recent Advances in Sensitized Photocathodes: From Molecular Dyes to Semiconducting Quantum Dots (Adv. Sci. 4/2018). *Adv. Sci.* **2018,** *5* (4), 1870023, DOI: https://doi.org/10.1002/advs.201870023.

(15) Gibson, E. A. Dye-Sensitized Photocathodes for H_2 Evolution. *Chem. Soc. Rev.* **2017,** *46* (20), 6194-6209, DOI: 10.1039/C7CS00322F.

(16) Nikolaou, V.; Charisiadis, A.; Charalambidis, G.; Coutsolelos, A. G.; Odobel, F. Recent Advances and Insights in Dye-Sensitized NiO Photocathodes for Photovoltaic Devices. *J. Mater. Chem. A* **2017,** *5* (40), 21077-21113, DOI: 10.1039/C7TA06500K.

(17) Lyu, S.; Massin, J.; Pavone, M.; Muñoz-García, A. B.; Labrugère, C.; Toupance, T.; Chavarot-Kerlidou, M.; Artero, V.; Olivier, C. H_2-Evolving Dye-Sensitized Photocathode Based on a Ruthenium–Diacetylide/Cobaloxime Supramolecular Assembly. *ACS Appl. Energy Matter.* **2019,** *2* (7), 4971-4980, DOI: 10.1021/acsaem.9b00652.

(18) Põldme, N.; O'Reilly, L.; Fletcher, I.; Portoles, J.; Sazanovich, I. V.; Towrie, M.; Long, C.; Vos, J. G.; Pryce, M. T.; Gibson, E. A. Photoelectrocatalytic H_2 Evolution from Integrated Photocatalysts Adsorbed on NiO. *Chem. Sci.* **2019,** *10* (1), 99-112, DOI: 10.1039/C8SC02575D.

(19) Windle, C. D.; Massin, J.; Chavarot-Kerlidou, M.; Artero, V. A Protocol for Quantifying Hydrogen Evolution by Dye-Sensitized Molecular Photocathodes and its Implementation for Evaluating a New Covalent Architecture Based on an Optimized Dye-Catalyst Dyad. *Dalton Trans.* **2018,** *47* (31), 10509-10516, DOI: 10.1039/C8DT01210E.

(20) Kaeffer, N.; Massin, J.; Lebrun, C.; Renault, O.; Chavarot-Kerlidou, M.; Artero, V. Covalent Design for Dye-Sensitized H_2-Evolving Photocathodes Based on a Cobalt Diimine–Dioxime Catalyst. *J. Am. Chem. Soc.* **2016,** *138* (38), 12308-12311, DOI: 10.1021/jacs.6b05865.

(21) Ji, Z.; He, M.; Huang, Z.; Ozkan, U.; Wu, Y. Photostable p-Type Dye-Sensitized Photoelectrochemical Cells for Water Reduction. *J. Am. Chem. Soc.* **2013,** *135* (32), 11696-11699, DOI: 10.1021/ja404525e.

(22) Pati, P. B.; Zhang, L.; Philippe, B.; Fernández-Terán, R.; Ahmadi, S.; Tian, L.; Rensmo, H.; Hammarström, L.; Tian, H. Insights into the Mechanism of a Covalently Linked Organic Dye–Cobaloxime Catalyst System for Dye-Sensitized Solar Fuel Devices. *ChemSusChem* **2017,** *10* (11), 2480-2495, DOI: 10.1002/cssc.201700285.

(23) Kaeffer, N.; Windle, C. D.; Brisse, R.; Gablin, C.; Leonard, D.; Jousselme, B.; Chavarot-Kerlidou, M.; Artero, V. Insights into the Mechanism and Aging of a Noble-Metal Free H_2-Evolving Dye-Sensitized Photocathode. *Chem. Sci.* **2018,** *9* (32), 6721-6738, DOI: 10.1039/C8SC00899J.

(24) Creissen, C. E.; Warnan, J.; Reisner, E. Solar H_2 Generation in Water with a $CuCrO_2$ Photocathode Modified with an Organic Dye and Molecular Ni Catalyst. *Chem. Sci.* **2018,** *9* (6), 1439-1447, DOI: 10.1039/C7SC04476C.

(25) Antila, L. J.; Ghamgosar, P.; Maji, S.; Tian, H.; Ott, S.; Hammarström, L. Dynamics and Photochemical H_2 Evolution of Dye–NiO Photocathodes with a Biomimetic FeFe-Catalyst. *ACS Energy Lett.* **2016,** *1* (6), 1106-1111, DOI: 10.1021/acsenergylett.6b00506.

(26) Li, F.; Xu, R.; Nie, C.; Wu, X.; Zhang, P.; Duan, L.; Sun, L. Dye-Sensitized $LaFeO_3$ Photocathode for Solar-Driven H_2 Generation. *Chem. Commun.* **2019,** *55* (86), 12940-12943, DOI: 10.1039/C9CC06781G.

(27) Creissen, C. E.; Warnan, J.; Antón-García, D.; Farré, Y.; Odobel, F.; Reisner, E. Inverse Opal $CuCrO_2$ Photocathodes for H_2 Production Using Organic Dyes and a Molecular Ni Catalyst. *ACS Catal.* **2019,** *9* (10), 9530-9538, DOI: 10.1021/acscatal.9b02984.

(28) Gross, M. A.; Creissen, C. E.; Orchard, K. L.; Reisner, E. Photoelectrochemical Hydrogen Production in Water using a Layer-by-Layer Assembly of a Ru Dye and Ni Catalyst on NiO. *Chem. Sci.* **2016,** *7* (8), 5537-5546, DOI: 10.1039/C6SC00715E.

(29) Shan, B.; Das, A. K.; Marquard, S.; Farnum, B. H.; Wang, D.; Bullock, R. M.; Meyer, T. J. Photogeneration of Hydrogen from Water by a Robust Dye-Sensitized Photocathode. *Energy Environ. Sci.* **2016,** *9* (12), 3693-3697, DOI: 10.1039/C6EE02903E.

(30) Shan, B.; Sherman, B. D.; Klug, C. M.; Nayak, A.; Marquard, S. L.; Liu, Q.; Bullock, R. M.; Meyer, T. J. Modulating Hole Transport in Multilayered Photocathodes with Derivatized p-Type Nickel Oxide and Molecular Assemblies for Solar-Driven Water Splitting. *J. Phys. Chem. Lett.* **2017,** *8* (18), 4374-4379, DOI: 10.1021/acs.jpclett.7b01911.

(31) Wang, D.; Sheridan, M. V.; Shan, B.; Farnum, B. H.; Marquard, S. L.; Sherman, B. D.; Eberhart, M. S.; Nayak, A.; Dares, C. J.; Das, A. K.; Bullock, R. M.; Meyer, T. J. Layer-by-Layer Molecular Assemblies for Dye-Sensitized Photoelectrosynthesis Cells Prepared by Atomic Layer Deposition. *J. Am. Chem. Soc.* **2017,** *139* (41), 14518-14525, DOI: 10.1021/jacs.7b07216.

(32) Materna, K. L.; Beiler, A. M.; Thapper, A.; Ott, S.; Tian, H.; Hammarström, L. Understanding the Performance of NiO Photocathodes with Alkyl-Derivatized Cobalt Catalysts and a Push–Pull Dye. *ACS Appl. Mater. Interfaces* **2020,** *12* (28), 31372-31381, DOI: 10.1021/acsami.0c05228.

(33) Wood, C. J.; Summers, G. H.; Clark, C. A.; Kaeffer, N.; Braeutigam, M.; Carbone, L. R.; D'Amario, L.; Fan, K.; Farre, Y.; Narbey, S.; Oswald, F.; Stevens, L. A.; Parmenter, C. D. J.; Fay, M. W.; La Torre, A.; Snape, C. E.; Dietzek, B.; Dini, D.; Hammarstrom, L.; Pellegrin, Y.; Odobel, F.; Sun, L.; Artero, V.; Gibson, E. A. A Comprehensive Comparison of Dye-Sensitized NiO Photocathodes for Solar Energy Conversion. *Phys. Chem. Chem. Phys.* **2016,** *18* (16), 10727-10738, DOI: 10.1039/C5CP05326A.

(34) Dillon, R. J.; Alibabaei, L.; Meyer, T. J.; Papanikolas, J. M. Enabling Efficient Creation of Long-Lived Charge-Separation on Dye-Sensitized NiO Photocathodes. *ACS Appl. Mater. Interfaces* **2017,** *9* (32), 26786-26796, DOI: 10.1021/acsami.7b05856.

(35) D'Amario, L.; Antila, L. J.; Pettersson Rimgard, B.; Boschloo, G.; Hammarström, L. Kinetic Evidence of Two Pathways for Charge Recombination in NiO-Based Dye-Sensitized Solar Cells. *J. Phys. Chem. Lett.* **2015,** *6* (5), 779-783, DOI: 10.1021/acs.jpclett.5b00048.

(36) Queyriaux, N.; Wahyuono, R. A.; Fize, J.; Gablin, C.; Wächtler, M.; Martinez, E.; Léonard, D.; Dietzek, B.; Artero, V.; Chavarot-Kerlidou, M. Aqueous Photocurrent Measurements Correlated to Ultrafast Electron Transfer Dynamics at Ruthenium Tris Diimine Sensitized NiO Photocathodes. *J. Phys. Chem. C* **2017,** *121* (11), 5891-5904, DOI: 10.1021/acs.jpcc.6b12536.

(37) Charisiadis, A.; Giannoudis, E.; Pournara, Z.; Kosma, A.; Nikolaou, V.; Charalambidis, G.; Artero, V.; Chavarot-Kerlidou, M.; Coutsolelos, A. G. Synthesis and Characterization of a Covalent Porphyrin-Cobalt Diimine-Dioxime Dyad for Photoelectrochemical H_2 Evolution. *Eur. J. Inorg. Chem.* **2021,** *2021* (12), 1122-1129, DOI: https://doi.org/10.1002/ejic.202001111.

(38) Bold, S.; Massin, J.; Giannoudis, E.; Koepf, M.; Artero, V.; Dietzek, B.; Chavarot-Kerlidou, M. Spectroscopic Investigations Provide a Rationale for the Hydrogen-Evolving Activity of Dye-Sensitized Photocathodes Based on a Cobalt Tetraazamacrocyclic Catalyst. *ACS Catal.* **2021,** *11* (6), 3662-3678, DOI: 10.1021/acscatal.0c05033.

(39) Queyriaux, N.; Giannoudis, E.; Lefebvre, J.-F.; Artero, V.; Chavarot-Kerlidou, M. Synthesis of Ruthenium Tris-Diimine Photosensitizers Substituted by Four Methylphosphonate Anchoring Groups for Dye-Sensitized Photoelectrochemical Cell Applications. *Eur. J. Inorg. Chem.* **2019,** *2019* (15), 2154-2161, DOI: 10.1002/ejic.201900151.

(40) Kaeffer, N.; Chavarot-Kerlidou, M.; Artero, V. Hydrogen Evolution Catalyzed by Cobalt Diimine–Dioxime Complexes. *Acc. Chem. Res.* **2015,** *48* (5), 1286-1295, DOI: 10.1021/acs.accounts.5b00058.

(41) Natu, G.; Hasin, P.; Huang, Z.; Ji, Z.; He, M.; Wu, Y. Valence Band-Edge Engineering of Nickel Oxide Nanoparticles via Cobalt Doping for Application in p-Type Dye-Sensitized Solar Cells. *ACS Appl. Mater. Interfaces* **2012,** *4* (11), 5922-9, DOI: 10.1021/am301565j.

(42) Queyriaux, N.; Andreiadis, E. S.; Torelli, S.; Pecaut, J.; Veldkamp, B. S.; Margulies, E. A.; Wasielewski, M. R.; Chavarot-Kerlidou, M.; Artero, V. CuAAC-Based Assembly and Characterization of a Ruthenium–Copper Dyad Containing a Diimine–Dioxime Ligand Framework. *Faraday Discuss.* **2017,** *198* (0), 251-261, DOI: 10.1039/C6FD00204H.

(43) Andreiadis, E. S.; Jacques, P.-A.; Tran, P. D.; Leyris, A.; Chavarot-Kerlidou, M.; Jousselme, B.; Matheron, M.; Pécaut, J.; Palacin, S.; Fontecave, M.; Artero, V. Molecular Engineering of a Cobalt-Based Electrocatalytic Nanomaterial for H_2 Evolution under Fully Aqueous Conditions. *Nature Chem.* **2013,** *5* (1), 48-53.

(44) Baron, A.; Herrero, C.; Quaranta, A.; Charlot, M.-F.; Leibl, W.; Vauzeilles, B.; Aukauloo, A. Click Chemistry on a Ruthenium Polypyridine Complex. An Efficient and Versatile Synthetic Route for the Synthesis of Photoactive Modular Assemblies. *Inorg. Chem.* **2012,** *51* (11), 5985-5987, DOI: 10.1021/ic300227j.

(45) de Miguel, G.; Wielopolski, M.; Schuster, D. I.; Fazio, M. A.; Lee, O. P.; Haley, C. K.; Ortiz, A. L.; Echegoyen, L.; Clark, T.; Guldi, D. M. Triazole Bridges as Versatile Linkers in Electron Donor–Acceptor Conjugates. *J. Am. Chem. Soc.* **2011,** *133* (33), 13036-13054, DOI: 10.1021/ja202485s.

(46) Zieschang, F.; Schreck, M. H.; Schmiedel, A.; Holzapfel, M.; Klein, J. H.; Walter, C.; Engels, B.; Lambert, C. Photoinduced Electron Transfer Dynamics in Triarylamine–Naphthalene Diimide Cascades. *J. Phys. Chem. C* **2014,** *118* (48), 27698-27714, DOI: 10.1021/jp5085058.

(47) Bold, S.; Zedler, L.; Zhang, Y.; Massin, J.; Artero, V.; Chavarot-Kerlidou, M.; Dietzek, B. Electron Transfer in a Covalent Dye–Cobalt Catalyst Assembly – a Transient Absorption Spectroelectrochemistry Perspective. *Chem. Commun.* **2018,** *54* (75), 10594-10597, DOI: 10.1039/C8CC05556D.

(48) Ameline, D.; Diring, S.; Farre, Y.; Pellegrin, Y.; Naponiello, G.; Blart, E.; Charrier, B.; Dini, D.; Jacquemin, D.; Odobel, F. Isoindigo Derivatives for Application in p-Type Dye Sensitized Solar Cells. *RSC Advances* **2015,** *5* (104), 85530-85539, DOI: 10.1039/C5RA11744E.

(49) Roy, S.; Bacchi, M.; Berggren, G.; Artero, V. A Systematic Comparative Study of Hydrogen-Evolving Molecular Catalysts in Aqueous Solutions. *ChemSusChem* **2015,** *8* (21), 3632-3638, DOI: 10.1002/cssc.201501002.

(50) Hawecker, J.; Lehn, J. M.; Ziessel, R. Efficient Homogeneous Photochemical Hydrogen Generation and Water Reduction Mediated by Cobaloxime or Macrocyclic Cobalt Complexes. *New J. Chem.* **1983,** *7* (5), 271-277.

(51) Fihri, A.; Artero, V.; Razavet, M.; Baffert, C.; Leibl, W.; Fontecave, M. Cobaloxime-Based Photocatalytic Devices for Hydrogen Production. *Angew. Chem. Int. Ed.* **2008,** *47* (3), 564-567.

(52) In the absence of the cobalt catalyst, the small amount of hydrogen produced might come from the photoelectroreduction of electrically disconnected NiO nanoparticles, as previously reported by A. N. Simonov and coworkers for a related organic dye-sensitized photocathode (see *J. Phys. Chem. C*, **2017**, *121*, 25836-25846).

(53) Of note, under these conditions, TEOA is employed as a sacrificial electron donor to generate the reduced dye via the reductive quenching of its excited state.

(54) Smolentsev, G.; Cecconi, B.; Guda, A.; Chavarot-Kerlidou, M.; van Bokhoven, J. A.; Nachtegaal, M.; Artero, V. Microsecond X-ray Absorption Spectroscopy Identification of Co^{I} Intermediates in Cobaloxime-Catalyzed Hydrogen Evolution. *Chem. Eur. J.* **2015,** *21* (43), 15158-15162, DOI: 10.1002/chem.201502900.

(55) Zhang, P.; Jacques, P.-A.; Chavarot-Kerlidou, M.; Wang, M.; Sun, L.; Fontecave, M.; Artero, V. Phosphine Coordination to a Cobalt Diimine-Dioxime Catalyst Increases Stability during Light-Driven H_2 Production. *Inorg. Chem.* **2012,** *51* (4), 2115-2120, DOI: 10.1021/ic2019132.

(56) Adler, D.; Feinleib, J. Electrical and Optical Properties of Narrow-Band Materials. *Phys. Rev. B* **1970,** *2* (8), 3112-3134, DOI: 10.1103/PhysRevB.2.3112.

(57) Boschloo, G.; Hagfeldt, A. Spectroelectrochemistry of Nanostructured NiO. *J. Phys. Chem. B* **2001,** *105* (15), 3039-3044, DOI: 10.1021/jp003499s.

(58) Föhlinger, J.; Maji, S.; Brown, A.; Mijangos, E.; Ott, S.; Hammarström, L. Self-Quenching and Slow Hole Injection May Limit the Efficiency in NiO-Based Dye-Sensitized Solar Cells. *J. Phys. Chem. C* **2018,** *122* (25), 13902-13910, DOI: 10.1021/acs.jpcc.8b01016.

(59) Herrero, C.; Batchelor, L.; Baron, A.; El Ghachtouli, S.; Sheth, S.; Guillot, R.; Vauzeilles, B.; Sircoglou, M.; Mallah, T.; Leibl, W.; Aukauloo, A. Click Chemistry as a Convenient Tool for the Incorporation of a Ruthenium Chromophore and a Nickel–Salen Monomer into a Visible-Light-Active Assembly. *Eur. J. Inorg. Chem.* **2013,** *2013* (4), 494-499, DOI: 10.1002/ejic.201201161.

(60) Sheth, S.; Baron, A.; Herrero, C.; Vauzeilles, B.; Aukauloo, A.; Leibl, W. Light-Induced Tryptophan Radical Generation in a Click Modular Assembly of a Sensitiser-Tryptophan Residue. *Photochem. Photobiol. Sci.* **2013,** *12* (6), 1074-1078, DOI: 10.1039/C3PP50021G.

(61) Herrero, C.; Quaranta, A.; El Ghachtouli, S.; Vauzeilles, B.; Leibl, W.; Aukauloo, A. Carbon Dioxide Reduction via Light Activation of a Ruthenium-Ni(Cyclam) Complex. *Phys. Chem. Chem. Phys.* **2014,** *16* (24), 12067-12072, DOI: 10.1039/C3CP54946A.

(62) Herrero, C.; Quaranta, A.; Sircoglou, M.; Senechal-David, K.; Baron, A.; Marin, I. M.; Buron, C.; Baltaze, J.-P.; Leibl, W.; Aukauloo, A.; Banse, F. Successive Light-Induced Two Electron Transfers in a Ru-Fe Supramolecular Assembly: From Ru-Fe(II)-OH_2 to Ru-Fe(IV)-oxo. *Chem. Sci.* **2015,** *6* (4), 2323-2327, DOI: 10.1039/C5SC00024F.

(63) Tebo, A. G.; Quaranta, A.; Herrero, C.; Pecoraro, V. L.; Aukauloo, A. Intramolecular Photogeneration of a Tyrosine Radical in a Designed Protein. *ChemPhotoChem* **2017,** *1* (3), 89-92, DOI: https://doi.org/10.1002/cptc.201600044.

(64) Gardner, J. M.; Beyler, M.; Karnahl, M.; Tschierlei, S.; Ott, S.; Hammarström, L. Light-Driven Electron Transfer between a Photosensitizer and a Proton-Reducing Catalyst Co-adsorbed to NiO. *J. Am. Chem. Soc.* **2012,** *134* (47), 19322-19325, DOI: 10.1021/ja3082268.

(65) Kamire, R. J.; Majewski, M. B.; Hoffeditz, W. L.; Phelan, B. T.; Farha, O. K.; Hupp, J. T.; Wasielewski, M. R. Photodriven Hydrogen Evolution by Molecular Catalysts using Al_2O_3-protected perylene-3,4-dicarboximide on NiO electrodes. *Chem. Sci.* **2017,** *8* (1), 541-549, DOI: 10.1039/C6SC02477G.

(66) Steinmetzer, J.; Kupfer, S.; Gräfe, S. pysisyphus: Exploring Potential Energy Surfaces in Ground and Excited States. *Int. J. Quantum Chem.* **2021,** *121* (3), e26390, DOI: https://doi.org/10.1002/qua.26390.

(67) Bhattacharjee, A.; Andreiadis, E. S.; Chavarot-Kerlidou, M.; Fontecave, M.; Field, M. J.; Artero, V. A Computational Study of the Mechanism of Hydrogen Evolution by Cobalt(Diimine-Dioxime) Catalysts. *Chem. Eur. J.* **2013,** *19* (45), 15166-15174, DOI: 10.1002/chem.201301860.

(68) Solis, B. H.; Yu, Y.; Hammes-Schiffer, S. Effects of Ligand Modification and Protonation on Metal Oxime Hydrogen Evolution Electrocatalysts. *Inorg. Chem.* **2013,** *52* (12), 6994-6999, DOI: 10.1021/ic400490y.

(69) Fang, D.; Zhang, Z.-Y.; Shangguan, Z.; He, Y.; Yu, C.; Li, T. (Hetero)arylazo-1,2,3-triazoles: "Clicked" Photoswitches for Versatile Functionalization and Electronic Decoupling. *J. Am. Chem. Soc.* **2021**, DOI: 10.1021/jacs.1c08704.

(70) Natali, M.; Campagna, S.; Scandola, F. Photoinduced Electron Transfer across Molecular Bridges: Electron- and Hole-Transfer Superexchange Pathways. *Chem. Soc. Rev.* **2014,** *43* (12), 4005-4018, DOI: 10.1039/C3CS60463B.

(71) Koch, A.; Kinzel, D.; Dröge, F.; Gräfe, S.; Kupfer, S. Photochemistry and Electron Transfer Kinetics in a Photocatalyst Model Assessed by Marcus Theory and Quantum Dynamics. *J. Phys. Chem. C* **2017,** *121* (30), 16066-16078, DOI: 10.1021/acs.jpcc.7b02812.

(72) Gillaizeau-Gauthier, I.; Odobel, F.; Alebbi, M.; Argazzi, R.; Costa, E.; Bignozzi, C. A.; Qu, P.; Meyer, G. J. Phosphonate-Based Bipyridine Dyes for Stable Photovoltaic Devices. *Inorg. Chem.* **2001,** *40* (23), 6073-6079, DOI: 10.1021/ic010192e.

(73) Hanson, K.; Brennaman, M. K.; Luo, H.; Glasson, C. R. K.; Concepcion, J. J.; Song, W.; Meyer, T. J. Photostability of Phosphonate-Derivatized, RuII Polypyridyl Complexes on Metal Oxide Surfaces. *ACS Appl. Mater. Interfaces* **2012,** *4* (3), 1462-1469, DOI: 10.1021/am201717x.

(74) We observed that all ions are detected as singly-charged species, irrespective of their expected charge; this was previously reported in the literature for ruthenium tris-diimine complexes analyzed by MALDI (see: F. M. MacDonnell and coll. *J. Am. Chem. Soc*. **1997**, *119*, 10364-10369; B. M. Tissue and coll. *Rapid Commun. Mass Spectrom*. **2001**, *15*, 1334-1340) and was attributed to the formation of protonated fully reduced complexes under these conditions of analysis.

(75) Queyriaux, N.; Jane, R. T.; Massin, J.; Artero, V.; Chavarot-Kerlidou, M. Recent Developments in Hydrogen Evolving Molecular Cobalt(II)–Polypyridyl Catalysts. *Coord. Chem. Rev.* **2015,** *304–305*, 3-19, DOI: http://dx.doi.org/10.1016/j.ccr.2015.03.014.

(76) Queyriaux, N.; Giannoudis, E.; Windle, C. D.; Roy, S.; Pécaut, J.; Coutsolelos, A. G.; Artero, V.; Chavarot-Kerlidou, M. A Noble Metal-Free Photocatalytic System Based on a Novel Cobalt Tetrapyridyl Catalyst for Hydrogen Production in Fully Aqueous Medium. *Sustainable Energy & Fuels* **2018,** *2* (3), 553-557, DOI: 10.1039/C7SE00428A.

(77) Tong, L.; Duan, L.; Zhou, A.; Thummel, R. P. First-Row Transition Metal Polypyridine Complexes that Catalyze Proton to Hydrogen Reduction. *Coord. Chem. Rev.* **2020,** *402*, 213079, DOI: https://doi.org/10.1016/j.ccr.2019.213079.

(78) Queyriaux, N.; Sun, D.; Fize, J.; Pécaut, J.; Field, M. J.; Chavarot-Kerlidou, M.; Artero, V. Electrocatalytic Hydrogen Evolution with a Cobalt Complex Bearing Pendant Proton Relays: Acid Strength and Applied Potential Govern Mechanism and Stability. *J. Am. Chem. Soc.* **2020,** *142* (1), 274-282, DOI: 10.1021/jacs.9b10407.

(79) Nie, C.; Liu, C.; Gong, L.; Wang, M. Boosting the Performance of a Silicon Photocathode for Photoelectrochemical Hydrogen Production by Immobilization of a Cobalt Tetraazamacrocyclic Catalyst. *J. Mater. Chem. A* **2021,** *9* (1), 234-238, DOI: 10.1039/D0TA09942B.

(80) Hanson, K.; Losego, M. D.; Kalanyan, B.; Parsons, G. N.; Meyer, T. J. Stabilizing Small Molecules on Metal Oxide Surfaces Using Atomic Layer Deposition. *Nano Lett.* **2013,** *13* (10), 4802-4809, DOI: 10.1021/nl402416s.

(81) Materna, K. L.; Jiang, J.; Crabtree, R. H.; Brudvig, G. W. Silatrane Anchors for Metal Oxide Surfaces: Optimization for Potential Photocatalytic and Electrocatalytic Applications. *ACS Appl. Mater. Interfaces* **2019,** *11* (6), 5602-5609, DOI: 10.1021/acsami.8b04138.

(82) Materna, K. L.; Lalaoui, N.; Laureanti, J. A.; Walsh, A. P.; Rimgard, B. P.; Lomoth, R.; Thapper, A.; Ott, S.; Shaw, W. J.; Tian, H.; Hammarström, L. Using Surface Amide Couplings to Assemble Photocathodes for Solar Fuel Production Applications. *ACS Appl. Mater. Interfaces* **2020,** *12* (4), 4501-4509, DOI: 10.1021/acsami.9b19003.

Table Of Contents (TOC) graphic: